EVIDENCE FOR MANGANESE-CATALYZED NITROGEN CYCLING IN SALT MARSH SEDIMENTS

A Thesis
Presented to
The Academic Faculty

by

Jennifer Denise Newton

In Partial Fulfillment
of the Requirements for the Degree
Master of Science in the
School of Earth and Atmospheric Sciences

Georgia Institute of Technology
May 2006

EVIDENCE FOR MANGANESE-CATALYZED NITROGEN CYCLING IN SALT MARSH SEDIMENTS

Approved by:

Dr. Martial Taillefert, Advisor
School of Earth and Atmospheric Sciences
Georgia Institute of Technology

Dr. Ellery Ingall
School of Earth and Atmospheric Sciences
Georgia Institute of Technology

Dr. Thomas DiChristina
School of Biology
Georgia Institute of Technology

Date Approved: April 10, 2006

ACKNOWLEDGEMENTS

This thesis is a compilation of effort from many people, of whom I wish to thank. First, I would like to thank my advisor, Dr. Martial Taillefert, for all his help and guidance over the last two and a half years. His never-ending support and discussions from the beginning were invaluable through every step in this project. I also wish to express my many thanks to my thesis committee, Dr. Ellery Ingall and Dr. Thomas DiChristina, for their constructive criticism and helpful insights. Further, I would like to thank Dr. Ellery Ingall for access to his lab and instruments and for the group discussions in connecting his group's work with mine. Thank you to Meg Grantham for all her endless help with the GFAAS, especially through the software updates. Many thanks go to Cynthia Vance-Harris for her many hours of instruction and help on the MIMS. Thank you to Hunter Oates who analyzed some of my samples in the beginning and taught me the colorimetric method for ammonium. I could not have completed this work without the support, in and out of the lab, of the members of our lab group: Beth Carey and Stephanie Chow for their untiring help in learning our methods, Gwen Bristow for her many appreciated opinions and vent sessions in our carpool and for staying up with me until 4:00 am processing my core, and to everyone else for all our laughs together. Finally, I dedicate this thesis to my family. My many thanks go to my mother who has always stood by me through all my life decisions. And, to my husband Donovan, thank you for all of your support and strength, without which I would not be where I am today.

TABLE OF CONTENTS

LIST OF TABLES

Page

LIST OF FIGURES

Page

SUMMARY

Fixed nitrogen is important as nutrient for organic matter formation and as electron donor (nitrification) and acceptor (denitrification) for energy generation, but it is scarcely available in aquatic systems. Nitrification oxidizes ammonium to nitrite and nitrate. Denitrification uses these fixed species to form dinitrogen gas. The classic understanding of the nitrogen cycle requires dissolved oxygen for nitrification and anaerobic conditions for a denitrification pathway that reduces nitrate through various intermediates. The global nitrogen budget is imbalanced with more marine denitrification measured than estimated in the classic nitrogen cycle, suggesting alternative pathways exist. One alternative denitrification pathway is anammox, which directly oxidizes ammonium to dinitrogen with nitrite as the electron acceptor. Other alternative pathways for both nitrification and denitrification involve redox metals as catalysts. Manganese-catalyzed anaerobic nitrification and denitrification are thermodynamically favorable at neutral pH. However, experimental evidence for these processes is still lacking. This investigation seeks to uncover evidence of manganese-catalyzed nitrification and denitrification in salt marsh sediments.

Batch reactors with anaerobic sediment slurries from a salt marsh in coastal Georgia were incubated in the presence and absence of colloidal manganese oxides and isotope-labeled ammonium and nitrate to trace dinitrogen formation. Ammonium removal in the manganese-treated reactors is accompanied by a high nitrite production compared to the nitrogen-only treatment, indicating manganese-catalyzed nitrification exists. Results show that denitrification is more prominent in the manganese-treated

reactors and that the classic heterotrophic denitrification pathway may not be substantial in shallow salt marsh sediments. These data indicate that anammox and/or manganese-coupled denitrification are major contributors to the removal of nitrite and nitrate.

These data show that manganese may play a role in the cycling of nitrogen in salt marsh sediments. Primary productivity is generally high in salt marshes, but oxygen penetrates less than a few millimeters in the sediment. Therefore, these observations suggest that oxygenic nitrification does not fuel denitrification below the sediment-water interface. Manganese-catalyzed nitrification allows formation of nitrite and nitrate in otherwise oxygen-limited sediments. The global nitrogen budget may be better constrained by incorporating these manganese-catalyzed anaerobic pathways. Though these processes will not completely balance the nitrogen cycle alone, evidence for manganese-catalyzed nitrogen cycling indicates that other redox-active metals, such as iron, could also contribute to nitrification and denitrification pathways.

CHAPTER 1

INTRODUCTION

Fixed nitrogen is an important nutrient in the global system both for energy and organic matter generation. The cycling of nitrogen is then essential to understand. Fixed nitrogen includes ammonium (NH_4^+), nitrate (NO_3^-) and nitrite (NO_2^-). NO_3^- and NO_2^- are formed through nitrification, the process of oxidizing NH_4^+, classically requiring oxygen (Hulth et al. 1999). Ammonium-oxidizing bacteria reduce oxygen to transform ammonium into nitrite (Madigan et al. 2003):

$$NH_4^+ + \frac{3}{2}O_2 \rightarrow NO_2^- + H_2O + 2H^+ \qquad (1.1)$$

While Eq. 1.1 is the overall reaction involved in formation of nitrite, it is a simplistic and slightly deceiving view. Bacteria cannot directly oxidize ammonium. Ammonium must first be activated in the cells before oxidation. For nitrite formation, NH_4^+ is activated to hydroxylamine (NH_2OH) by ammonia monooxygenase (AMO) through O_2 reduction. NH_2OH is oxidized to NO_2^- by hydroxylamine oxidoreductase, releasing electrons to cytochromes. The cytochromes divide the electrons with two transported to reduce another O_2 to H_2O and two transported to AMO to complete the cycle. The oxidation steps release H^+, which are pumped to ATPase to form ATP.

Nitrite-oxidizing bacteria then reduce oxygen to oxidize nitrite to nitrate (Madigan et al. 2003):

$$NO_2^- + \frac{1}{2}O_2 \rightarrow NO_3^- \qquad (1.2)$$

Similarly, Eq. 1.2 is also a simplistic view of nitrite oxidation. First, NO_2^- is oxidized to NO_3^- by nitrite oxidoreductase (NOR). The electrons are pumped through cytochromes to reduce O_2 to H_2O. H^+ is pumped to ATPase to form ATP.

As a result of nitrification reactions, sediment profiles of nitrate and nitrite display maximum concentration at the oxic/anoxic interface and an exponential decrease with depth (Thamdrup and Dalsgaard 2000). These exponential profile decreases are attributed to the removal of nitrite and nitrate through heterotrophic denitrification (Froelich et al. 1979, Thamdrup and Dalsgaard 2000).

Ammonium and nitrate are also integrated into organic matter through assimilation (Madigan et al. 2003). Growth by organisms requires nitrogen (ammonium and nitrate) which is incorporated in biomass.

Denitrification is the pathway through the electron transport chain that reduces nitrate to dinitrogen through a series of intermediate nitrogen compounds (Madigan et al. 2003). Nitrate is first reduced to nitrite with the nitrate reductase, and then further reduced to nitrogen monoxide, nitrous oxide, and finally dinitrogen gas, each step corresponding to its own reductase protein (Madigan et al. 2003). The dinitrogen gas recirculates into the nitrogen cycle through nitrogen fixation – the reduction of dinitrogen gas back to ammonium.

Nitrogen fixation is not the only pathway for NH_4^+ production. Ammonification is the pathway of NH_4^+ release into solution from organic matter degradation (Madigan et al. 2003). Also, NH_3 is produced through anaerobic respiration on NO_2^- (Takeuchi 2006, Mohan et al. 2004). NH_4^+ sediment profiles show NH_4^+ production at depth with the production attributed mainly to ammonification. The entire classic nitrogen cycle is represented in **Figure 1.1**.

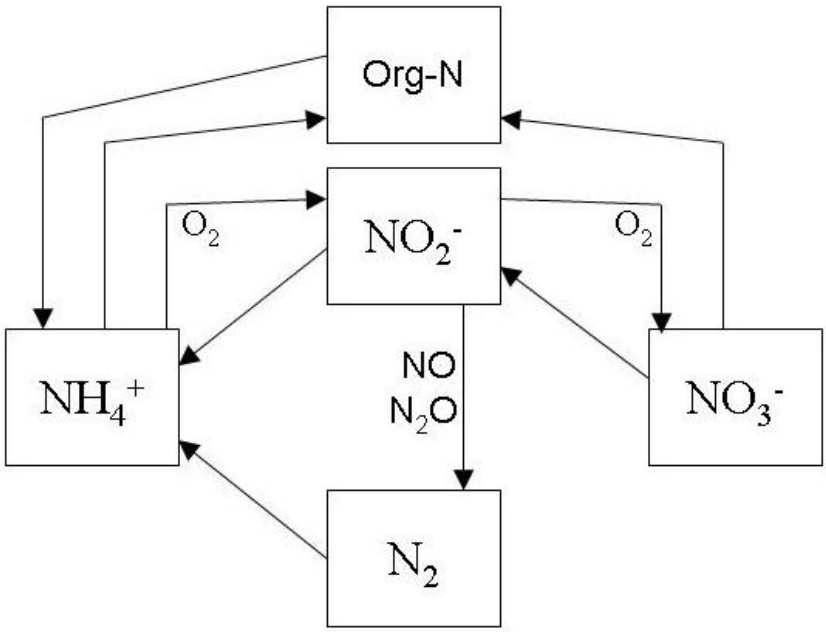

Figure 1.1: The classic nitrogen cycle. NO_3^- is produced solely through oxidation by O_2. The oxidation of NH_4^+ to NO_2^- and NO_2^- to NO_3^- occur in different organisms. Denitrification requires the NO_3^- to reduce back to NO_2^- before following the rest of the classic denitrification chain. The entire denitrification process occurs in a single organism. Reduction of NO_2^- to NH_4^+ is assumed as anaerobic respiration on NO_2^-.

In the classic nitrogen cycle, a global nitrogen budget can be calculated from rates measured in incubated sediment for nitrification (Sutka et al. 2004; Welsh and Castadelli 2004) and denitrification (Devol et al. 1997; Jones et al. 2000) and reservoir sizes from measured concentrations in pore water profiles (Froelich et al 1979; Anschutz et al. 2000; Thamdrup and Dalsgaard 2000; Deflandre et al. 2002) and ocean water column (Plus et al. (2003)). From these calculations, the nitrogen budget is imbalanced. Higher denitrification rates and lower concentrations of NO_x^- in the global oceans are measured than accounted for by the nitrogen budget (Middelburg et al. 1996). This imbalance implies that alternative pathways must exist in the nitrogen cycle.

One such pathway that was recently discovered is anammox – anaerobic ammonium oxidation (**Figure 1.2**). The anammox process consists of bacteria that

oxidize ammonium directly to N_2 using NO_2^- or NO_3^- as the electron donor (Jetten et al. 1999):

$$NH_4^+ + NO_2^- \rightarrow N_2 + 2H_2O \quad (1.3)$$

$$\frac{5}{3}NH_4^+ + NO_3^- \rightarrow \frac{4}{3}N_2 + 3H_2O + \frac{2}{3}H^+ \quad (1.4)$$

Similar to the nitrification processes, Eq. 1.3 and 1.4 are only net reactions occurring in the anammox organisms. For Eq. 1.3, NH_3 combines with NH_2OH to form hydrazine (N_2H_4) and H_2O by hydrazine hydrolase (HH). N_2H_4 is oxidized to N_2 releasing H^+ and electrons through hydrazine oxidoreductase (HZO). H^+ is pumped to ATPase to form ATP, and the electrons are pumped to nitrite reductase to reduce NO_2^- to NH_2OH to complete the cycle.

Nitrite is the preferred oxidized nitrogen species for anammox, since is requires a simple one to one ratio between ammonium and nitrite, but the nitrate pathway is also prominent in marine sediments (Thamdrup and Dalsgaard 2002). The process was first discovered in wastewater treatment plants when ammonium was disappearing from an anaerobic denitrifying bed reactor (Mulder et al. 1995). It was soon after discovered to happen in coastal ocean and continental shelf sediments and water column (Kuypers et al. 2003; Dalsgaard et al. 2003; Vance-Harris and Ingall 2005) and marine estuaries (Trimmer et al. 2003; Risgaard-Petersen et al. 2004).

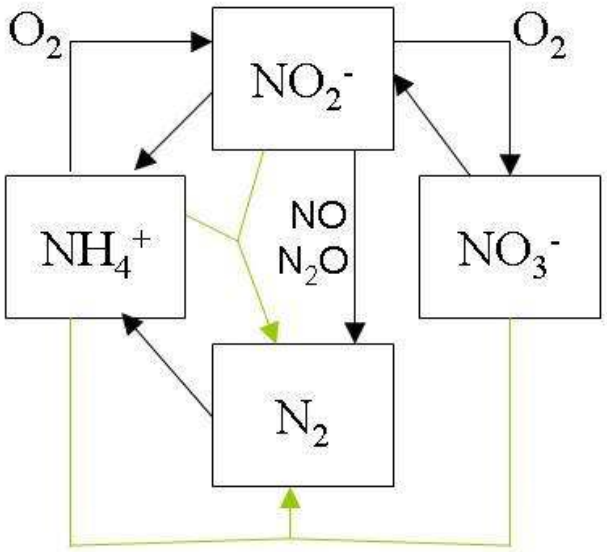

Figure 1.2: The classic nitrogen cycle plus anammox. The two known anammox reactions are labeled by green arrows, while the classic nitrogen cycle is in black.

Another alternative pathway hypothesized is redox metal (Fe and Mn) catalysis of nitrification and denitrification. Thermodynamically, Fe and Mn could be used by autotrophic organisms to reduce nitrate (Luther et al. 1997) and expand the number of organisms that could denitrify:

$$NO_3^- + 5Fe^{2+} + 12H_2O \rightarrow \frac{1}{2}N_2 + 5Fe(OH)_3 + 9H^+ \quad (1.5)$$

$$NH_4^+ + \frac{3}{2}MnO_2 + 2H^+ \rightarrow N_2 + \frac{3}{2}Mn^{2+} + 3H_2O \quad (1.6)$$

$$NO_3^- + \frac{5}{2}Mn^{2+} + 2H_2O \rightarrow \frac{1}{2}N_2 + \frac{5}{2}MnO_2 + 4H^+ \quad (1.7)$$

In addition, thermodynamics show that nitrification processes could also be catalyzed by Mn (Luther et al. 1997) in nitrifying bacteria. The interest in Mn-catalyzed nitrification is that nitrification could occur anaerobically:

$$4MnO_2 + NH_4^+ + 6H^+ \rightarrow 4Mn^{2+} + NO_3^- + 5H_2O \quad (1.8)$$

$$MnO_2 + NO_2^- + 2H^+ \rightarrow Mn^{2+} + NO_3^- + H_2O \quad (1.9)$$

Iron coupling (Eq. 1.5) has already been discovered in freshwater sediments (Straub et al. 1996; Straub et al. 1998) through isolation of bacterial strains and incubations, but evidence is still lacking for manganese coupling to the nitrogen cycle. A schematic diagram of nitrification and denitrification catalyzed by manganese is shown in **Figure 1.3**.

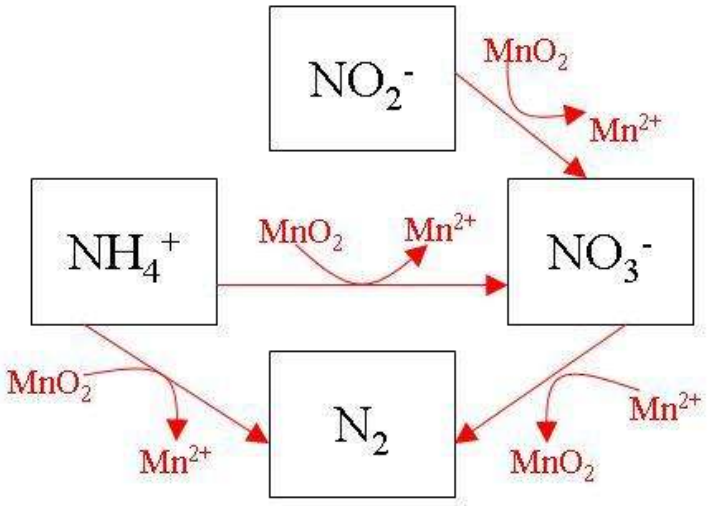

Figure 1.3: Schematic diagram of proposed Mn-catalyzed reactions involved in nitrogen cycling. All reactions are labeled with the corresponding reduction or oxidation of Mn species. All catalyzed reactions couple to Mn reduction except denitrification from NO_3^-.

Possible evidence for anaerobic nitrification appears in sediment depth profiles. Anschutz et al. (2000) used microelectrodes to measure redox metal species (Mn and Fe) and oxygen with high spatial resolution. These profiles show oxygen removal in the first 5-10 mm of sediment. NO_2^- and NO_3^-, measured after pore water extraction demonstrated high concentrations near the sediment-water interface (SWI) and exponential decreases that mimic the oxygen profile. Nitrate and nitrite reappeared deeper at high concentrations. Since the second nitrogen maximum correlated with a peak in Mn^{2+} concentrations, the authors hypothesized that this could be evidence for the

alternative Mn-catalyzed nitrification. Deflandre et al. (2002) found the same features – high NO_2^- and NO_3^- at the surface, an exponential decrease, and new peaks correlating with Mn^{2+} peaks at depth in anoxic sediments of the Saguenay Fjord in the St. Lawrence estuary.

Sediment incubations were also conducted to investigate metal catalysis in marine sediments. Hulth et al. (1999) ran different types of incubations on sediment taken from Long Island Sound, USA, searching for the Mn-catalyzed nitrification pathway. The first experiment was a "closed anoxic incubation" (Martens and Berner 1974), in which collected sediment was first mixed with and without a concentration of solid MnO_2, and then added to air-tight sealed jars. The jars were sealed in plastic bags and immersed in anoxic sediments. The other experiment was a "diffusively open" incubation (Aller and Mackin 1989), in which plugs of sediment were open to constantly degassing anoxic sea water allowing exchange between the overlying water and the sediment. No additions of manganese and nitrogen were included in the overlying water.

The closed incubations demonstrated more direct evidence of anoxic nitrification, since the only electron acceptor added was the solid MnO_2. Results of the "diffusively open" incubations were more ambiguous, as different terminal electron acceptors were available in the overlying water. Because the data are not based solely on the shape and correlation of sediment profiles, these results are more direct evidence for Mn-catalyzed nitrification than the previously published pore water profiles (Anschutz et al. 2000, Deflandre et al. 2002).

The only other incubations published for anoxic nitrification are the incubations of Thamdrup and Dalsgaard (2000). Cores were measured for geochemical profiles, and

anoxic sediment was incubated in gas-tight NEN/PE plastic bags using different inoculations. One was amended with nitrate, one with ammonium, and one with ammonium and solid MnO_2. The bags were closed with no headspace and sealed in a dinitrogen atmosphere. Thamdrup and Dalsgaard (2000) did not find evidence of anoxic nitrification in their incubations, but they speculated that the sediment composition, with the measured and added MnO_2, and ammonium concentration were different enough from Hulth et al. (1999) to change the conditions for Mn-catalysis.

All of the manganese-catalyzed nitrification and denitrification reactions (Eq. 1.6 – 1.9) are thermodynamically favorable at all pH values, but the specific nitrification reaction (Eq. 1.8) is only favorable at a pH value below 7.8 (Luther et al. 1997). Ocean water has an average pH of 8.00, above the thermodynamically favorable zone, but most surface waters and pore waters of coastal sediments have lower pHs, suggesting that Eq. 1.8 is favorable. For example, Kostka et al. (2002) and Bull and Taillefert (2001) measured pH values ranging between 6.0 and 7.5 in salt marsh sediments. Of course, thermodynamics is not the only factor controlling the probability of reaction. Biological mediation could allow thermodynamically unfavorable reactions to proceed.

The organisms known to cycle nitrogen classically could also potentially cycle nitrogen through alternative pathways. For example, the accepted mechanisms in the first step of nitrification– oxidation of NH_4^+ to NO_2^- – use oxygen where the redox half reaction:

$$\frac{1}{4}O_2 + H^+ + e^- \rightarrow \frac{1}{2}H_2O \qquad (1.10)$$

has an electron potential of +0.81 V at pH 7 at standard state (Nordstrom and Munoz 1994). The alternative first nitrification step uses manganese reduction where the redox half reaction:

$$\frac{1}{2}MnO_2 + 2H^+ + e^- \rightarrow \frac{1}{2}Mn^{2+} + H_2O \quad (1.11)$$

has an electron potential of +0.46 V at pH 7 at standard state (Nordstrom and Munoz 1994). The classic ammonium oxidation step:

$$\frac{1}{6}NH_4^+ + \frac{1}{3}H_2O \rightarrow \frac{1}{6}NO_2^- + e^- + \frac{4}{3}H^+ \quad (1.12)$$

requires +0.34V (Madigan et al. 2003). Since Mn reduction contributes a high enough electron potential for the initial nitrification mechanism, ammonium-oxidizing bacteria could contain the machinery to contribute to anaerobic nitrification:

$$\frac{1}{2}MnO_2 + \frac{1}{6}NH_4^+ + \frac{2}{3}H^+ \rightarrow \frac{1}{2}Mn^{2+} + \frac{1}{6}NO_2^- + \frac{2}{3}H_2O \quad (1.13)$$

In an oxic environment, the bacteria would preferentially reduce oxygen as in classic nitrification, but in anoxic conditions, manganese is also a viable option, since it still contributes more energy than required for oxidation of ammonium to nitrite.

Mortimer et al. (2004) characterized different ammonia oxidizing bacteria throughout a sediment core from a fjord in Scotland searching for evidence of ammonia oxidizers at depth in anoxic sediments. Pore water profiles revealed similar results to Anschutz et al. (2000) and Deflandre et al. (2002) with NO_2^- and NO_3^- decreasing exponentially from the surface, then peaking again at depth in anoxic sediment. 16S RNA analyses showed strong signals for the various organisms, indicating diverse communities of ammonia oxidizing bacteria throughout the sediment profile. The process was repeated on several cores with the same result. The ammonia oxidizing

community composition stayed roughly the same in the profile regardless of oxygen limitations.

Similar to the ammonium oxidizers above, the formal nitrifiers oxidize nitrite to nitrate. Also similar to the ammonium oxidizing bacteria, nitrifiers use the electron transport chain to oxidize nitrite to nitrate and reduce oxygen to water. Just as before, oxygen reduction has a higher electron potential of +0.81 V compared to +0.46 V for manganese reduction, but both are still higher than the energy needed for nitrite oxidation at standard state (+0.43 V):

$$\frac{1}{2}NO_2^- + \frac{1}{2}H_2O \rightarrow \frac{1}{2}NO_3^- + e^- + H^+ \quad (1.14)$$

From the redox potentials, it appears that manganese can be used as the oxidant of nitrite in anaerobic sediments. The kinetics of this reaction was studied chemically by Luther and Popp (2002) with the conclusion that it is unfavorable above a pH of 5. These data confirm that this process must be biologically mediated.

In this study, metal-catalyzed nitrification and denitrification reactions were investigated in sediment incubations to find definitive evidence of manganese influence in the nitrogen cycle. Salt marsh sediments were selected according to the distribution of redox chemical species involved and incubated in sealed batch tube reactors to find evidence for Mn-catalyzed nitrification and denitrification. It was found that nitrate and nitrite were produced anaerobically, and their production is correlated to the reduction of Mn-oxides. Also, denitrification was more significant in sediments inoculated with Mn-oxides than sediments without Mn-oxides. These experiments provide the first evidence for the nature of Mn-catalyzed nitrogen cycling. These conclusions could be used to balance the nitrogen budget with alternative pathways.

CHAPTER 2

EXPERIMENTAL DESIGN

Field measurements were conducted to select the best sediment layers for this study. Incubations were performed using the optimal sediment to find evidence for Mn-catalyzed nitrogen cycling.

2.1 Study Site

All sediment used in this study was collected from the Skidaway Institute of Oceanography (SkIO) salt marsh in Savannah, Georgia. **Figure 2.1** shows a map of the area, including all locations for mud and core collection used in this study: shallow sediment from summer of 2004 at the main tidal creek bank by Ellery Ingall's laboratory group (Earth and Atmospheric Sciences, Georgia Tech), deeper sediment from summer of 2004 in a small tributary tidal creek, and shallow sediment from summer of 2005 at the main tidal creek bank.

2.2 Evidence of N-Mn Coupling from Sediment Profiles

A sediment core from the SKIO salt marsh was taken in June 2005 at the end of the boardwalk on the main tidal creek bank to find evidence of nitrification at depth (**Figure 2.1**). The core was first processed voltammetrically then sliced to extract porewaters. The core was sliced with 0.5 cm resolution in a glovebag under an anaerobic N_2 atmosphere. Each slice was centrifuged in 50 mL polypropylene Falcon tubes (Fisher). The porewaters were separated for different analyses to be conducted back in the lab. One mL of each porewater sample was acidified with 200 μL of 1 M HCl (Fisher) and refrigerated for Mn_d analysis. Two mL was frozen immediately for NH_4^+, NO_2^-, and NO_3^- analyses.

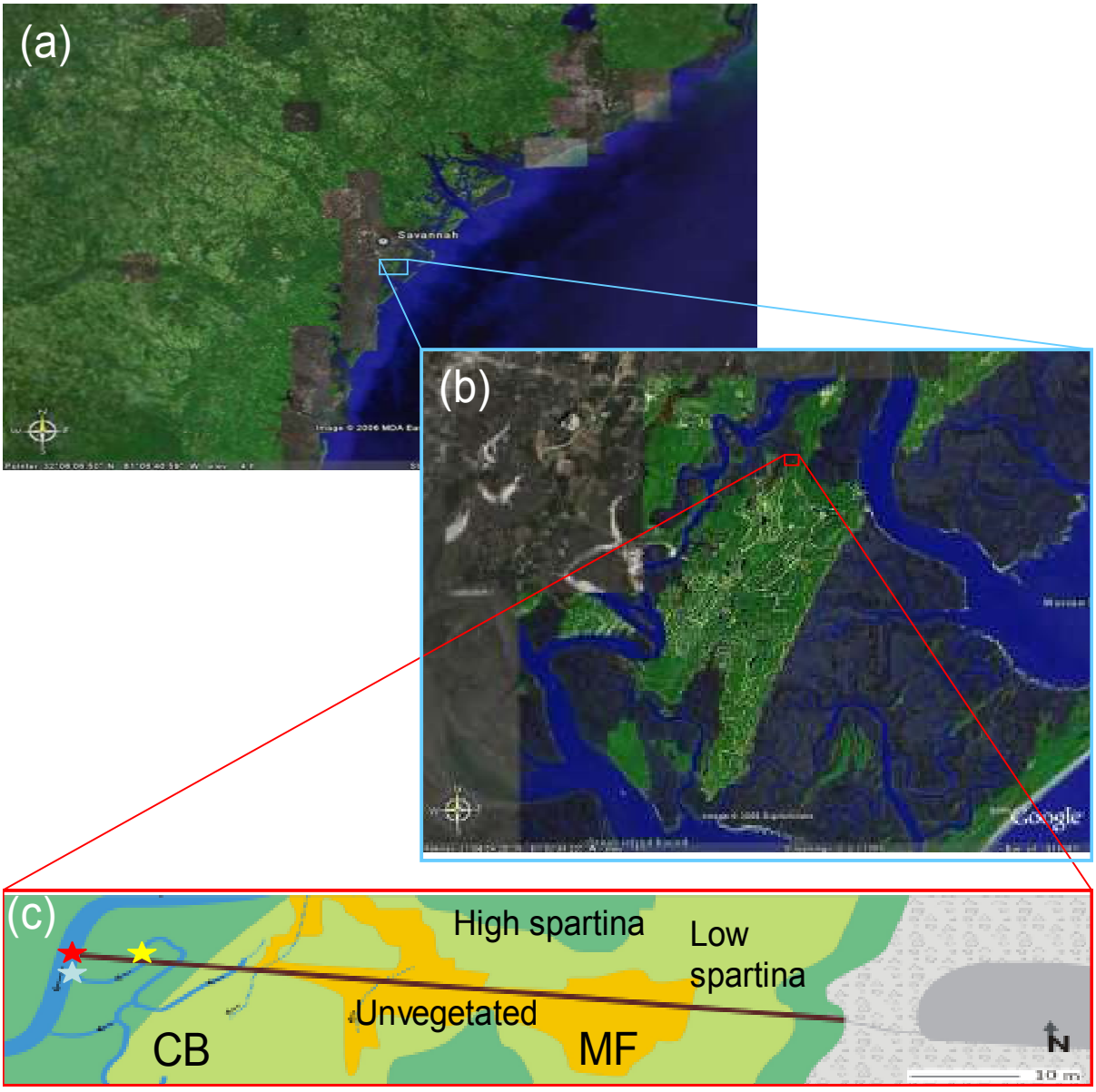

Figure 2.1: (a) Map of Skidaway Island (blue box) in relation to Savannah and the Georgia coast. (b) Close up of Skidaway Island indicated in red. (c) View of the salt marsh study area with the locations of the sediment sampled in this study. A boardwalk runs from the eastern freshwater inland to to the main tidal creek bank to the west. The dark green regions indicate dense spartina grass; the light green regions indicate low spartina grass; and the yellow indicates areas without vegetation. The area is characterized by two different environments – the mud flat (MF) and the creek bank (CB). All sediments taken for this study came from CB. The blue star indicates the location of sediment for the test incubation. The red star indicates the shallow sediment location. The yellow star indicates the deeper sediment location.

2.3 Salt Marsh Sediment Incubations

In order to determine the importance of Mn in the cycling of nitrogen, sediment was incubated under varying conditions in batch tube reactors (BTR, total volume = 25 mL). The tubes and rubber stoppers were first triple acid-washed in trace-metal grade 2% HCl (Fisher), then labeled and weighed. The tubes and stoppers were autoclaved (Consolidated Stills and Sterilizers) to minimize biological contamination. Between 3 and 5 mL of wet sediment was filled into a 5 mL syringe (Henke Sass Wolf GMBH, luer lock) with the end previously cut (**Figure 2.2**).

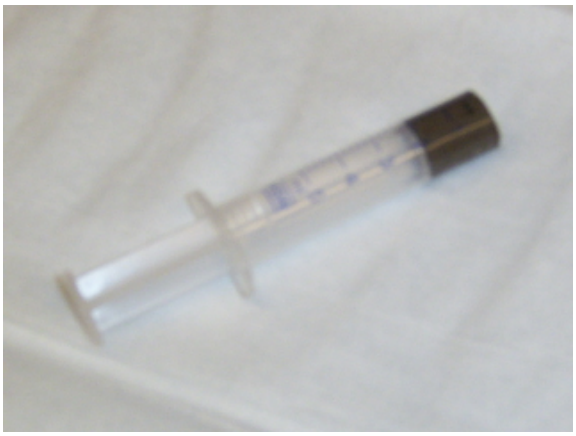

Figure 2.2: The 5 mL syringe with the end removed filled with 2 mL of sediment. Once the sediment was compressed into the syringe, it was injected into BTR.

The sediment was immediately injected into the BTR and closed with a rubber stopper. The tube was reweighed to determine the exact mass of wet sediment. Specific solutions of artificial sea water (ASW) diluted to the salinity of the salt marsh were added to the reweighed tubes. The tubes were mixed thoroughly for homogeneity of the sediment slurries in the beginning of the incubations, and the sediment was allowed to settle (**Figure 2.3**). All tubes were kept in the dark at room temperature (**Figure 2.4**) until extracted.

The solution consisted of artificial marsh water (AMW) amended with NH_4^+ and/or $MnO_{2(c)}$. The artificial marsh water contained 55% ASW (**Table 2.1**) and 45% MilliQ water, giving a final salinity of 20 ‰. Colloidal manganese oxides were made to fix the form of Mn oxides added through the chemical reaction (Fisher; Perez-Benito and Arias 1992):

$$8KMnO_4 + 3Na_2S_2O_3 + 2H^+ \rightarrow 8MnO_{2(c)} + 6SO_4^{2-} + 6Na^+ + 8K^+ + H_2O \qquad (2.1)$$

Table 2.1: Artificial sea water (ASW) composition. This solution has a salinity of 36 ‰ and ionic strength of 0.73. ASW was diluted to make AMW.

ASW Species	Concentration
NaCl	0.43 M
Na_2SO_4	29 mM
KCl	11 mM
$MgCl_2 \cdot 6H_2O$	55 mM
$CaCl_2 \cdot 2H_2O$	11 mM
$NaHCO_3$	2.3 mM

During each extraction, the raw samples were measured first voltammetrically. All BTR samples were then filtered (0.2 μm polyethersulfone membrane, Whatman) and divided between refrigerated acidified and frozen unacidified vials for later analyses. Samples were acidified with 200 μL 1 M HCl in 1.3 mL sample and later measured for total dissolved Mn (Mn_d). Unacidified, frozen samples were measured for all dissolved N speciation (NH_4^+, NO_2^-, and NO_3^-).

Figure 2.3: Filled and sealed BTR in holding rack. Each numbered tube was weighed, autoclaved, and then reweighed with the wet sediment addition.

Figure 2.4: The holding rack was placed in a dark cabinet to avoid light interference. Each row of tubes corresponds to a different treatment.

2.3.1 Determination of Initial Concentrations

A test incubation was conducted to determine the optimal N : Mn ratio in the inoculum used in the incubations with the SkIO salt marsh sediment. BTR were filled with 5 mL sediment and 18 mL of solution. Sediment was collected in the summer of 2003 in the mouth of a small tributary tidal creek (**Figure 2.1**).

The initial ratios of NH_4^+ : $MnO_{2(c)}$ were randomly selected to cover a wide distribution of previously measured concentrations in these particular sediments. Initial bulk solutions of 2 mM NH_4Cl (Fisher) and 1 mM $MnO_{2(c)}$ (Eq. 2.1) were diluted into AMW to ratios of 0.1, 0.5, 0.8, 1.0, 2.0, 5.0, and 10, respectively. Samples were taken roughly once a week for 80 days. Before 1 mL of solution was extracted, the tubes were remixed for homogeneity of the solution, and the sediment was allowed to resettle. Mn^{2+}, total dissolved Mn (Mn_d), and NH_4^+ were the only species measured in these incubations.

2.3.2 Time Series Incubations – $MnO_{2(c)}$ + $^{15}NH_4^+$

Three replicate incubations were conducted over 50 – 65 days to determine Mn influence on N cycling. The same procedure for filling BTR was used but with 3 mL of sediment and 20 mL of solution. The inoculum consisted of 800 μM $^{15}NH_4Cl$ (Fisher) and 160 μM $MnO_{2(c)}$ in AMW. The ^{15}N labeling allowed the NH_4^+ contribution to be tracked to N_2 production through measurement of $^{29}N_2$ (^{15}N + ^{14}N) and $^{30}N_2$ (^{15}N + ^{15}N). Since the isotope analysis required a high volume of 10 – 15 mL of solution, two tubes were sacrificed for analysis roughly once a week for 50 days. One tube went for isotopic analysis, and the other was divided for the other dissolved and solid phase analyses. O_2, Mn^{2+}, Mn_d, adsorbed Mn^{2+} (Mn_{ads}), $^{29}N_2$, $^{30}N_2$, and NH_4^+ were measured for each sample for all three incubations.

Mn-catalysis was tested against the difference in redox zonations associated with depth. Two incubations used shallow tidal creek sediment, while one incubation used deeper tidal creek sediment (**Figure 2.1**). ΣNO_x^- was measured for each sample in one of

the shallow sediment incubations with collaboration from Ingall's laboratory. The other shallow incubation included 160 μM $MnO_{2(c)}$, 800 μM NH_4^+, and 50 μM $^{14}NO_3^-$ in the initial inoculum to trace heterotrophic denitrification (Section 2.3.4). The samples in this incubation were also measured for reactive amorphous Mn-oxides (Mn_s), and for distinction between NO_2^- and NO_3^-. The deeper tidal creek sediment did not include a NO_3^- inoculation, but did include measurements of NO_2^- and NO_3^-.

2.3.3 Incubations with $^{15}NH_4^+$ Only

Two incubations were also conducted to determine the nitrogen speciation in sediment slurry treatments without the addition of $MnO_{2(c)}$ in shallow and deep sediments – only 800 μM $^{15}NH_4^+$ in AMW was inoculated. The deeper sediments were from the tributary tidal creek bank, and the shallower sediments were from the main tidal creek bank (**Figure 2.1**). The deeper incubation included the same measurements as the deeper sediment $MnO_{2(c)}$ treatment. The shallower sediment incubation again included $^{14}NO_3^-$ to trace heterotrophic denitrification (Section 2.3.4) and all the same measurements as the $MnO_{2(c)}$ + $^{15}NH_4^+$ + $^{14}NO_3^-$ treatment.

2.3.4 Heterotrophic Denitrification Incubation

One incubation was conducted to test for heterotrophic denitrification in shallow salt marsh sediments. The treatment included 800 μM $^{14}NH_4^+$, 50 μM $^{15}NO_3^-$, and 160 μM $MnO_{2(c)}$ in AMW. The nitrogen isotopes were switched compared to the previous incubations to test for production of $^{30}N_2$ by heterotrophic denitrification ($^{15}NO_3^-$ + $^{15}NO_3^-$). The full N and Mn speciation was conducted including O_2, Mn^{2+}, Mn_d, Mn_{ads}, Mn_s, $^{29}N_2$, $^{30}N_2$, NH_4^+, NO_2^-, and NO_3^-.

2.3.5 Control Incubations

Each type of sediment, shallow and deeper tidal creek bank sediment, was tested for a background speciation in live control treatments. AMW was added to the wet sediment without additions of NH_4^+, NO_3^-, or $MnO_{2(c)}$. Full N and Mn speciations were conducted in both controls.

CHAPTER 3

METHODS

3.1 Solid Phase Extractions

Mn solid phases were extracted sequentially from the sediment. Adsorbed Mn (Mn_{ads}) was first extracted, and then followed by the reactive amorphous Mn oxides (Mn_s). All extractions were performed and measured in triplicate.

3.1.1 Adsorbed Manganese(II)

Mn_{ads} was measured by a simple ion exchange method (Tessier et al 1979). One molar $MgCl_2 \cdot 6H_2O$ (Fisher) in MilliQ water was used to release the Mn adsorbed on the sediment surface. Since Mg^{2+} has a higher affinity for sorbents than Mn^{2+}, it was assumed that after an equilibration time, all the Mn^{2+} was released by the exchange with excess Mg^{2+}:

$$\equiv S:Mn + Mg^{2+} \rightarrow Mn^{2+} + \equiv S:Mg \qquad (3.1)$$

The Mg^{2+} ion exchange technique also assumed that no $MnCO_{3(s)}$ was dissolved during the extraction process. Other exchangeable ion reagents, such as Na-acetate, may attack and dissolve carbonates while releasing the exchangeable ions, causing a higher, inaccurate, Mn_{ads} value (Tessier et al. 1979). Since the Mg^{2+} reaction is a simple ion exchange from loosely connected adsorbed species, the carbonates are left intact. Roughly 0.5 g of sediment was added to 10 mL of the exchange reagent. Samples were mixed overnight then centrifuged. The supernatant was acidified for later analysis of dissolved Mn (Mn_d).

3.1.2 Amorphous Manganese Oxides

Mn_s is measured by the same extraction process for Fe amorphous oxides. Since Fe and Mn have similar chemical properties, an ascorbate extraction will release the Fe and Mn from both metals' amorphous oxides (Anschutz et al 2000). The reagent used in the extraction contained first 0.2 M Na-citrate (tribasic – Sigma-Aldrich) and 0.6 M $NaHCO_3$. Twenty g L^{-1} L-ascorbic acid (Fisher) was added to reach a final pH of 8. The leftover supernatant from the Mn_{ads} extraction was removed from the samples before the second extraction. Ten mL of the ascorbate reagent was added, and the samples were mixed overnight then centrifuged. The supernatant was collected and immediately measured for Mn_d, since the reagent is buffered from acidification by the $NaHCO_3$.

3.2 Voltammetry

Voltammetric analyses were conducted to measure O_2, Mn^{2+}, Fe^{2+}, soluble-organic Fe^{3+}, and ΣH_2S in the batch tube reactor (BTR) supernatant. The strength of voltammetry is the ability of the electrodes to measure *in situ* all of the above species in one scan with high spatial resolution and low detection limits (Taillefert and Luther 2000). All measurements were conducted using an Analytical Instrument Systems (AIS) Model DLK-60 or Model DLK-100 potentiostat with Au/Hg solid-state amalgam microelectrodes as working electrodes (Brendel and Luther 1995). An Ag/AgCl electrode was used as the reference and a platinum wire was used as the counter electrode.

The Au/Hg solid-state microelectrodes consisted of a 100-μm diameter Au wire sealed in epoxy into a $^1/_8$" PEEK™ tube housing connected to the potentiostat by a copper conducting wire. The Au wire was polished sequentially with 15, 6, 1, and ¼ μm diamond paste to provide a smooth, flat surface to hold Hg. The electrode was then plated by reduction of Hg^{2+} at -0.1 V in a 0.1M $Hg(NO_3)_2$ solution in 2% HNO_3. The

electrode was finally polarized at -9 V for 90 seconds to provide an amalgam between the Au and Hg.

Measurements were made by applying a time-varying potential between the working and reference electrodes. The applied potential caused oxidation or reduction of different species at specific potentials (**Table 3.1**), and the resulting current was read at the counter electrode.

Table 3.1: Voltammetric half reactions and their reduction potentials at the Hg-plated gold wire surface (Brendel and Luther 1995).

Reactions	**E_p (V)**
$O_2 + 2H^+ + 2e^- + Hg \rightarrow H_2O_2(Hg)$	-0.30
$H_2O_2(Hg) + 2H^+ + 2e^- \rightarrow 2H_2O(Hg)$	-1.30
$HS^- + Hg \rightarrow HgS + H^+ + 2e^-$	< -0.60 (adsorption)
$HgS + H^+ + 2e^- \leftrightarrow HS^- + Hg$	-0.60
$Fe^{2+} + Hg + 2e^- \leftrightarrow Fe(Hg)$	-1.43
$org.Fe^{3+} + e^- + Hg \leftrightarrow Fe^{2+}(Hg)$	-0.2 to -0.9 (organic ligand dependent)
$Mn^{2+} + Hg + 2e^- \leftrightarrow Mn(Hg)$	-1.55

The result was a potential versus current scan, showing peaks in current at specific potentials representing different dissolved species (**Figure 3.1**). The specific voltammetric techniques used in this study included linear sweep voltammetry (LSV) for O_2 and H_2O_2 determination and cathodic square wave voltammetry (CSWV) for Mn^{2+}, Fe^{2+}, soluble-Fe^{3+}, and ΣH_2S ($H_2S + HS^- + S^{2-} + S^0 + S_x^{2-}$).

A sensitivity test for the microelectrodes was conducted using LSV to measure dissolved O_2 in artificial marsh water (AMW). A more sensitive electrode will produce a higher O_2 and H_2O_2 signal, giving a more defined O_2 curve, while a less sensitive

electrode will produce a lower signal and a less defined O_2 curve (**Figure 3.2**). A more O_2 sensitive electrode will generally produce a more sensitive CSWV calibration. The microelectrodes were first calibrated for O_2 using LSV in air-equilibrated AMW. The potential was applied, with a conditioning step of 10 s at -0.1 V, and scanned from -0.1 V to -1.75 V at a rate of 200 mV s^{-1}. The conditioning step cleaned the electrode surface, allowing more accuracy and reproducibility (Brendel and Luther 1995).

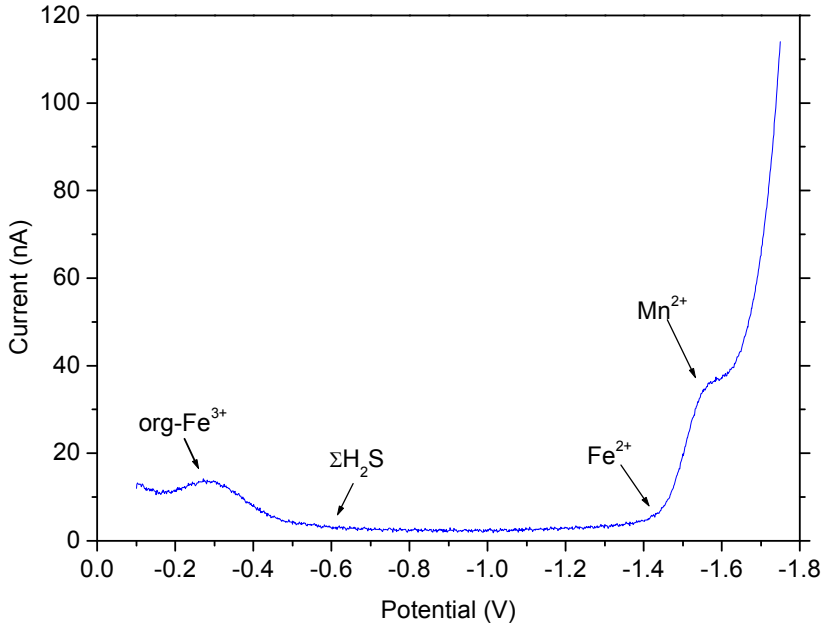

Figure 3.1: Sample voltammogram from one of the incubation samples. Only small amounts of Mn^{2+} and organic-Fe^{3+} were found in this sample. All four species of interest are labeled at their corresponding potentials.

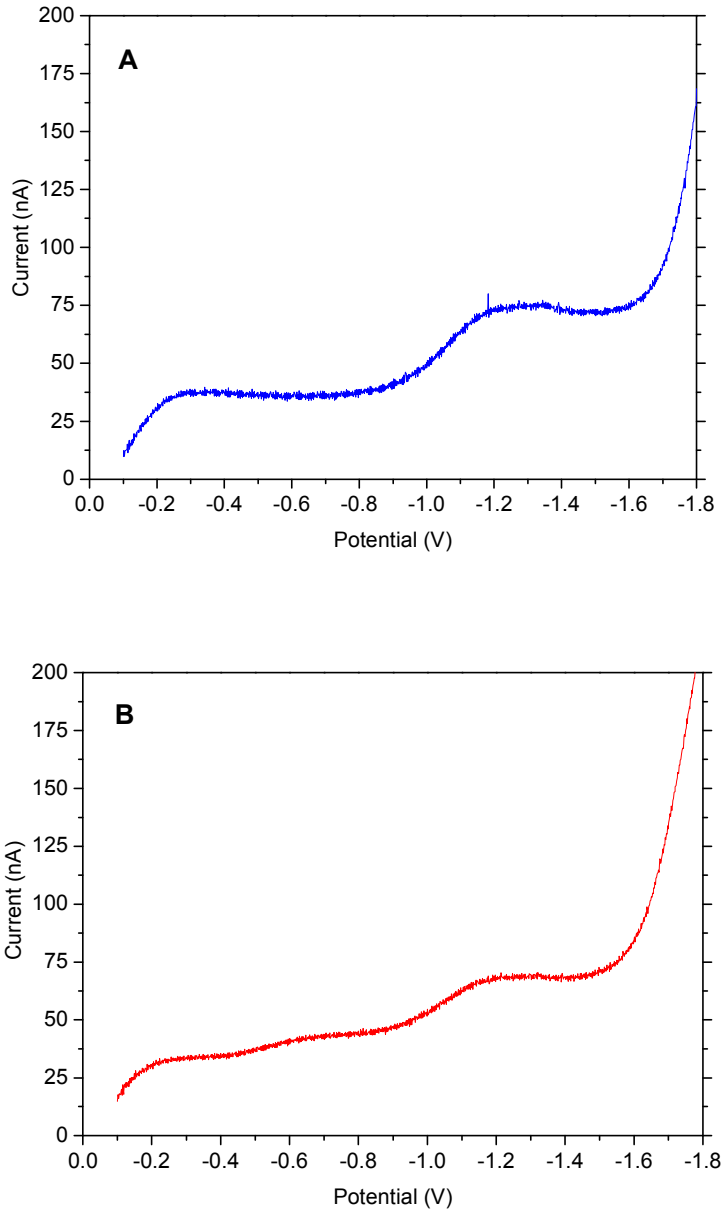

Figure 3.2: Sample voltammograms for linear sweep oxygen runs. (a) Sample of a well polished and plated PEEK™ electrode. The O_2 and H_2O_2 peaks are clear and distinct. (b) Sample of a poorly polished and plated PEEK™ electrode. The O_2 and H_2O_2 peaks are muffled and not easily determined.

Mn^{2+} calibration of the microelectrodes was conducted in degassed AMW with a stock solution of 0.1 M $MnCl_2 \cdot 4H_2O$ (Fisher) at pH 2 in MilliQ water (**Figure 3.3**). The Mn^{2+} voltammograms were obtained at the same potential range, scan rate, and conditioning step as the O_2 calibration runs. Increasing concentration of Mn^{2+} increases the current intensity. Voltammetry displays a linear relationship between current intensity and concentration (Brendel and Luther 1995), allowing for easy calibrations.

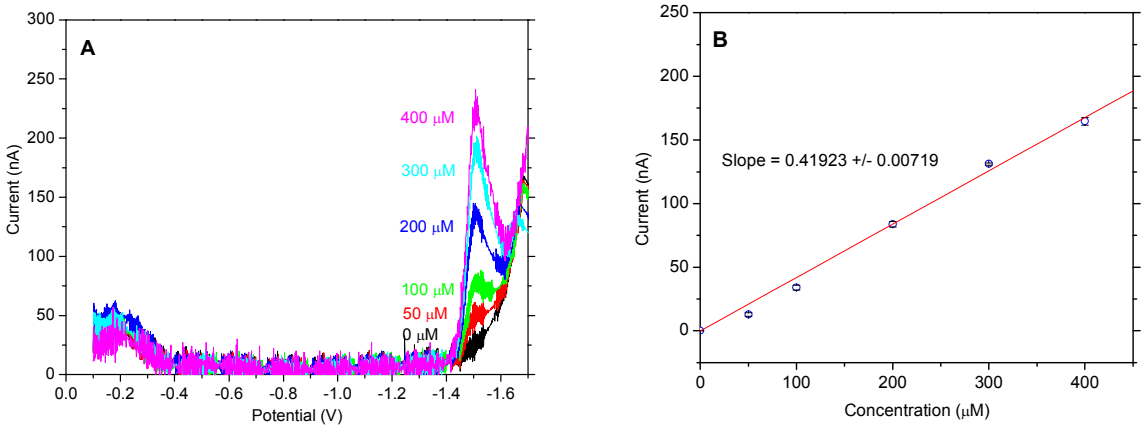

Figure 3.3: Mn calibration voltammograms and corresponding calibration curve. The most accurate detection limit of Mn^{2+} in seawater by microelectrode is around 50 µM, so the calibration varied from 50 to 400 µM, plus a blank. (a) Voltammograms for step-addition Mn calibration using volumes of $MnCl_2$ at pH = 2. Noise can interfere from external power surges or oversensitivity of the electrodes, though the integrated peaks still form a linear fit. (b) Calibration curve with 2σ standard deviation from voltammograms in (a). The noise from the runs did not interfere with the linearity of the curve. Reproducibility shows high precision with the PEEK™ electrodes.

Mn^{2+} is the only required calibration, since the concentrations of Fe^{2+} and ΣH_2S can be determined using the Pilot Ion technique (Brendel and Luther 1995). Replicate calibrations of the different species showed a relationship between the slopes of the Mn^{2+} calibration curve and the Fe^{2+} and ΣH_2S calibration curves. The slope of the Fe^{2+} calibration curve is equivalent to 0.36 times the Mn^{2+} calibration slope, and the CSWV sulfide calibration slope equals 12.6 times the Mn^{2+} calibration slope. Organic-soluble

Fe^{3+} concentrations can currently not be quantified, and org-Fe^{3+} is usually reported as the current intensity in nA.

For this study, the voltammetric measurements were conducted in the unacidifed, unfiltered sampling containers of the incubations' supernatant with no dilution since the concentrations of Mn^{2+} were below or within the calibration range. O_2 measurements were conducted immediately after the stoppers were removed to ensure anaerobic conditions were maintained throughout the incubations.

3.3 Ion Chromatography (IC)

IC measurements were conducted to determine concentrations of NO_2^- and NO_3^-. IC holds similar strengths to voltammetry, though the measurements are *ex situ*. IC also measures multiple species in one run at low detection limits, but through ion separation in a column. The method used was based on the method created by Rozan and Luther (2002). All measurements were performed with an ion chromatograph (Dionex, DX-300 Series) with an Alltech Anion/R 10 μm (150 x 4.6 mm) chromatography column and Alltech All-Guard Anion/R 7.5mm x 4.6 mm guard. The detector used was a Gilson 155 UV/Vis Detector with UV absorbance detection of 220 nm. Samples were pumped through a Dionex GP50 pump at 2 mL min^{-1} to the chromatography column where the NO_2^- and NO_3^- were separated before flowing to the detector.

The eluent used was 2.5 mM $NaClO_4$ (Sigma) in MilliQ water adjusted to pH 10. This eluent produced the best separation of peaks based on multiple trials. Lower pH values and higher $NaClO_4$ concentrations caused merging of the NO_2^- and NO_3^- peaks. The ClO_4^- eventually degrades and lowers the pH of the eluent if left for multiple days, so the solution was prepared fresh at least every 3 days as determined by consumption rates. Samples were detected at 220 nm with a sensitivity gain of 0.010 absorbance units to maximize the NO_2^- and NO_3^- peaks without causing significant Br^- interference. All seawater samples had to be diluted even in low NO_2^- and NO_3^- concentrations; Cl^-

concentrations appeared in the runs decreasing the sensitivity of the detector, and the high concentrations clogged the columns at a faster rate.

Combination standards from 0 to 40 μM were prepared using bulk solutions of 500 μM $NaNO_2$ and $NaNO_3$ (Fisher) in MilliQ water. Equivalent concentrations of NO_2^- and NO_3^- were added to each standard vial. In addition, equivalent amounts of AMW were added to create artificial salinity dilutions. The salt content also interfered in the NO_2^- and NO_3^- measurements, so the standards' salinity had to match the diluted samples. All concentrations were found using the unacidified samples diluted to 1:10 proportions. The dilution factor was suggested by Rozan and Luther (2002) for marine samples to decrease the Cl^- interference.

The detector read the absorbance of the samples over time and produced a time series with peaks for each species (**Figure 3.4**). Each species separates to a specific retention time based on charge affinity and size (**Table 3.2**). While each species does not follow an exact retention time, the species do cluster together around an average.

A test was also conducted to determine the possible interference of HS^- in pore water samples on the NO_2^- peaks. According to the test chromatograms in Rozan and Luther (2002), HS^- has a retention time less than half that of NO_2^- (6 min versus 14.5 min). This study's chromatograms show a retention time of roughly 6 min for NO_2^- (**Figure 3.4**), indicating potential HS^- interference from shorter retention times. A 10 μM NO_2^- solution was amended with varying concentrations of H_2S – between 0 and 20 μM. The resulting chromatograms indicate no interference up to 0.1 μM H_2S, the detection limit of H_2S using voltammetry. As voltammetric measurements were always performed before NO2- measurements, the sulfide interference could be documented.

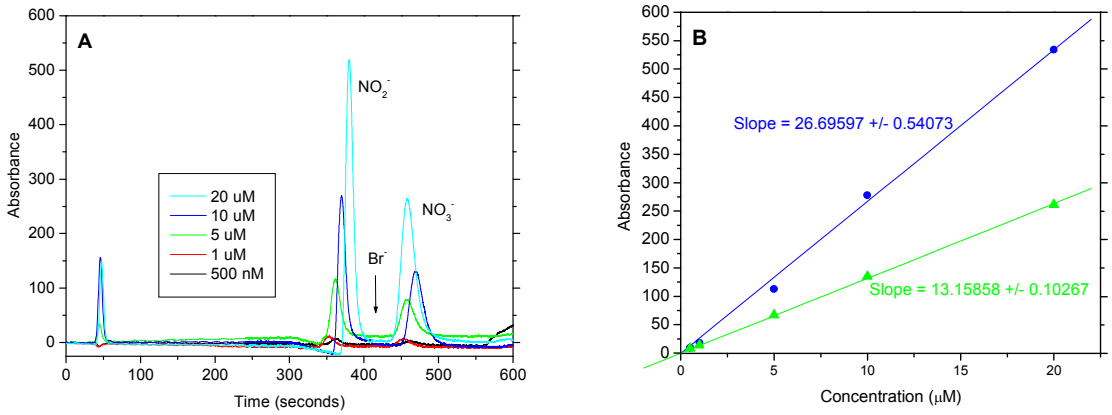

Figure 3.4: Absorbance spectra and corresponding calibration curve from the UV/Vis analysis on the IC. Eluent contains 2.5 mM $NaClO_4$ adjusted to pH 10. All standards are prepared in MilliQ water. (a) Absorbance spectra from a calibration IC run. The peaks for both NO_2^- and NO_3^- fall within a small area of retention times, with the retention times increasing with concentration. The arrow for Br^- indicates where the peak would fall if it was on the spectra. (b) Calibration curve from the spectra in (a).

Table 3.2: Average molar retention times and their 2σ standard deviations for all calibrations and samples in this study (150 samples). All runs were measured at 220 nm. Larger variations in retention times were caused by column condition or eluent age. The column was regenerated once during the study, and the eluent was changed at least every 3 days.

Species of Interest	**Retention Time (sec)**
NO_2^-	388.7 +/- 22.7
Br^-	411.7 +/- 29.9
NO_3^-	465.6 +/- 25.8

3.4 Membrane Inlet Mass Spectroscopy (MIMS)

The concentrations of $^{29}N_2$ and $^{30}N_2$ were measured on the MIMS as described in Kana et al. (1994) and adapted by Vance-Harris and Ingall (2005). Two seawater baths open to the atmosphere were used as the calibration points - one at 21°C and one at 30°C. The baths equilibrated for at least 24 hours. Liquid samples and standards were pumped through a gas permeable membrane located in a vacuum. Gases were then introduced into a quadrupole mass spectrometer to separate them by size before being read by the detector. Once the lines were opened, the machine was allowed to warm up and equilibrate for four hours with the intake line in MilliQ water before samples were analyzed. A peristaltic pump (IsmaTec®, Cole-Parmer Instrument Company) pumped the fluids – MilliQ water, standard water baths, and samples – from the intake line, through the system, and out the waste.

Once the MIMS was warmed up, water from the two seawater baths were introduced into the system. The standards were twice alternated with four measurements per injection. The samples were then analyzed with four measurements as well, with the input line inserted into the sample bottle immediately after the stopper was removed to minimize O_2 and $^{28}N_2$ contamination. The water from the standard baths was introduced again as before to account for instrument drift.

All concentrations were calculated using ratios of the N_2 species to Ar. Ar is not affected by biological processes, so it works well as a tracer for drift and environmental changes (temperature and salinity) compared to the species affected by biological processes. The standard water bath concentrations were found using the solubility of the species of interest at the salinity and temperature of the water. Sample concentrations of $^{29}N_2$ and $^{30}N_2$ were found using the calculations described in Kana et al. (1994) based on measurements of the standards.

3.5 Graphite Furnace Atomic Absorption Spectrophotometry (GFAAS)

Total dissolved Mn of the original supernatant and Mn concentrations of both solid-phase extractions were analyzed by GFAAS with Zeeman background corrections. The advantages of GFAAS include auto-calibration, auto-dilution of samples outside the calibration range, and an auto-sampler that requires small sample volumes (< 2 mL). During the course of this study, the Varian Spectra AA-600 received a software update, so two different standard techniques were needed. The older software required Mn standards between 0 and 50 nM. The newer software required Mn standards between 0 and 5 $\mu g\ L^{-1}$. All bulk standards were made using $MnCl_2 \cdot 4H_2O$ (Fisher) and trace metal grade HNO_3 (Fisher). Samples were diluted between 400 and 4000 times in trace metal 2% HNO_3 based on expected concentration of Mn_d in different treatments and Mn speciation.

3.6 Colorimetry

Concentrations of NH_4^+ were determined by colorimetric analysis based on Strickland and Parsons (1972). Measurements were conducted at 640 nm on a spectrophotometer (Milton Roy Spectronic 601) with standards of 0 to 20 μM made with a bulk standard of 100 μM NH_4Cl (Fisher) in MilliQ water. Reagents used included a phenol, a nitroprusside, and an alkaline solution. All reagent weights measured, reagent solutions added, and analyses done were conducted in a fume hood as a precaution. All bottles of reagents were parafilmed closed to prevent loss and health hazards. One molar phenol (Sigma) was dissolved in 100 mL of 95% ethanol (C_2H_5OH, ENG Scientific) and stored in a glass bottle. A 6 mM solution of the sodium nitroprusside, or sodium nitroferricyanide(III), ($Na_2[Fe(CN)_5\ NO] \cdot 2H_2O$, Aldrich) was mixed in MilliQ water and stored in a dark bottle. The alkaline reagent consisted of 0.7 M sodium citrate ($Na_3C_6H_5O_7 \cdot 2H_2O$, Sigma-Aldrich) and 0.25 M NaOH (Fisher) in 250 mL MilliQ water. All solutions were stable for months when stored in the refrigerator. Immediately before

the reagents were added to the standards and samples, 2.5 mL of 4-6% sodium hypochlorite (NaOCl, Fisher) was added to 10 mL of the alkaline reagent to create the oxidizing reagent. The reagents were added in a specific sequence: phenol first, nitroprusside second, and oxidizing reagent last. All vials were parafilmed, mixed, and heated in a 45°C oven for 1 hour before analysis. Unacidified, filtered supernatant samples were diluted in a 1:60 proportion for NH_4^+-added treatments and a 1:15 proportion for control treatments.

While the IC was under repair, ΣNO_x^- ($NO_2^- + NO_3^-$) was also measured in one of the incubations by colorimetric analysis by a partner laboratory group. The method was based on Strickland and Parsons (1972) using a Cd-Cu reduction column, sulphanilamide reagent, and N-(1-Naphythyl)-ethylenediamine dihydrochloride reagent. A separate NO_2^- analysis was not conducted, so only the combined concentration is known.

3.7 pH

The pH was measured in unfiltered samples with a pH/ISE meter (Orion, Model 290A*plus*). The potential and temperature of the samples were recorded and the pH calculated from the Nernst equation:

$$pH_{spl} = pH_{std} - \frac{(E_{spl} - E_{std})F}{2.303RT} \tag{3.2}$$

where E is the measured potentials for the samples (spl) and standard (std), F is Faraday's constant (96485.31 C mol^{-1}), R is the gas constant (8.3144 J mol^{-1} K^{-1}), and T is the temperature in K. A standard Tris buffer (pH = 8.28) in 0.54 M NaCl (Dickson 1993) was used for the calibration of this analysis.

CHAPTER 4

RESULTS

A tidal creek pore water profile from the salt marsh showed higher NO_2^- and NO_3^- concentrations both near the surface (7 μM for NO_3^- and NO_2^-) and at depth (3 μM for NO_3^- and 4.8 μM for NO_2^-, **Figure 4.1**). The sediment was anaerobic below the sediment-water interface (SWI). NH_4^+ was approximately 10 – 15 μM below the SWI before it was completely removed at a depth of 10 mm. NH_4^+ reappeared at a depth of 40 mm and peaked around 60 mm at a concentration of 60 μM before decreasing to the end of the profile. Mn^{2+} increased with depth to maximums at 10 mm (150 μM) and 40 mm (600 μM). Deeper in the sediment, Mn^{2+} stabilized at approximately 500 μM between 40 and 70 mm and approached the detection limit at the base of the core. The first Mn^{2+} maximum correlated to the first increase in fixed nitrogen. Fe^{2+} did not appear until after 40 mm and reached a maximum around 50 – 80 mm. The second Mn^{2+} maximum mirrored the Fe^{2+}profile. No sulfide was detected in the core.

This sediment was chosen for subsequent incubation experiments because of high Mn^{2+} concentrations and the presence of NH_4^+, NO_2^-, and NO_3^- at depth. The presence of deep NO_2^- and NO_3^- made the sediment a good potential candidate for the coupled N-Mn reactions (Eq. 1.6-1.8 and 1.13). Each of the incubations described in Chapter 2 was used to look for evidence of anaerobic nitrification and possible Mn-catalyzed nitrification and denitrification. All BTR incubations described in subsequent sections became suboxic within the first 10 days.

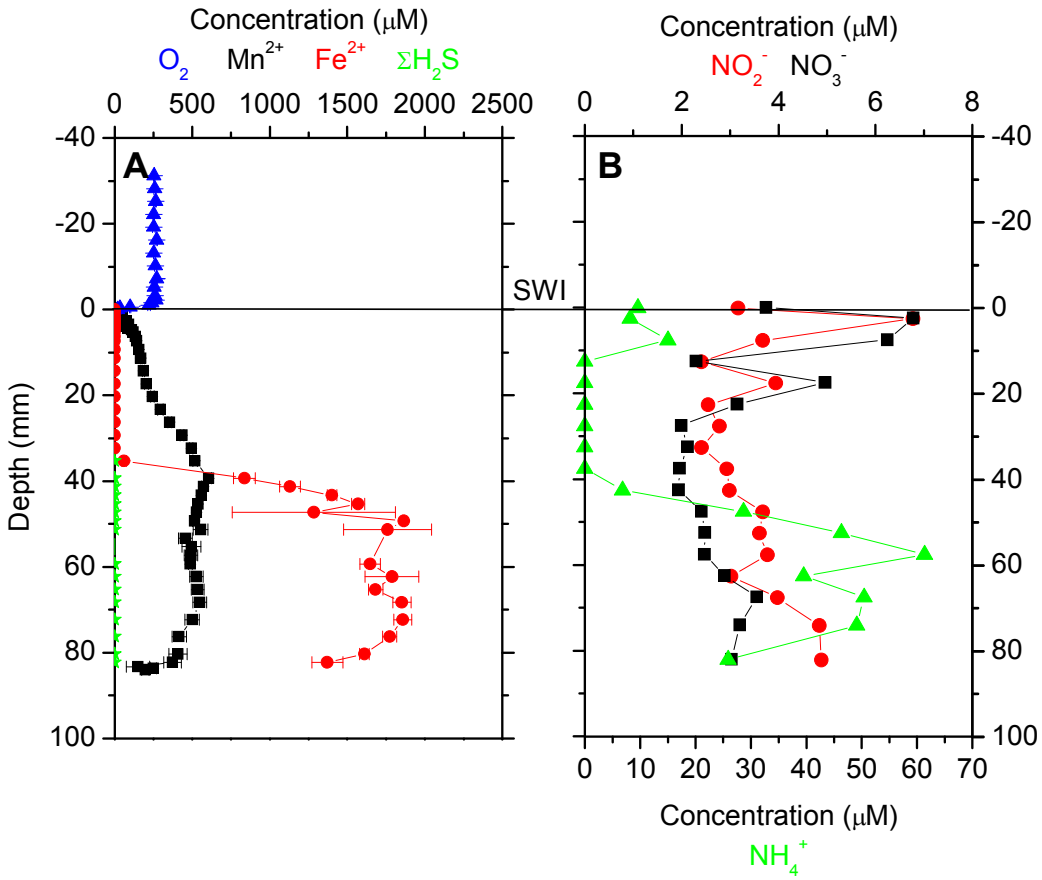

Figure 4.1: Profiles taken from a core on the main tidal creek bank (June 2005). The core was from the same location as the shallow incubation sediment. The sediment-water interface (SWI) is labeled in both profiles. (a) *Ex situ* voltammetric profile. O_2 reached 0 μM at SWI, indicating no O_2 influence at depth. Mn^{2+} was prominent at all depths below 5 mm in the sediment. Fe^{2+} appeared after 35 mm. No sulfide was detected. (b) Porewater profiles of the N species of interest. NO_2^- and NO_3^- peaked in anaerobic sediment around 10 – 20 mm and 50 – 80 mm.

4.1 Control Tests

The shallow (less than 10 cm) and deep (up to 20 cm) sediment from the creek banks were incubated in artificial marsh water (AMW) without the presence of nitrogen or metals as live controls. Both the shallow and the deep sediment slurry data revealed that production of NH_4^+ and fixed nitrogen reaches steady state quickly (**Figure 4.2** and **4.3**). Concentrations were similar to what was detected in sediments from this study (**Figure 4.1**) and the literature (Anschutz et al. 2000, Deflandre et al. 2002). The deep sediment (**Figure 4.2**) reached steady state concentrations of 80 μM for NH_4^+ and 40 μM for NO_3^-. No discernable NO_2^- was found. The speciation of Mn indicated that the processes regulating Mn distribution were not at steady state. Total dissolved Mn (Mn_d) appeared constant at 30 μM after the initial decrease over the first 14 days. However, Mn^{2+} was not detected until after 40 days. The shallow sediment control also contained low, steady state levels of all N and Mn species (**Figure 4.3**). Unlike the deep sediment, the shallow sediment incubations were measured for the isotope-enriched N_2 species and reactive amorphous Mn-oxides (Mn_s). The nitrogen species did not indicate a steady state system. The background N_2 values were above detection limits at 3 μM for both $^{29}N_2$ and $^{30}N_2$. NH_4^+ and NO_3^- were again low with concentrations around 80 μM and 0 μM, respectively, with an 80 mM peak of NO_3^- at 22 days. NO_2^- had a high maximum background concentration of 90 μM. The dissolved Mn species remained low in concentration: Mn_d concentrations stayed at roughly 50 μM, Mn^{2+} concentrations never reached 20 μM. In contrast, solid Mn species were significant: adsorbed Mn^{2+} (Mn_{ads}) slowly decreased from 0.4 to 0.2 μmol g^{-1} over the 56 day time span while Mn_s jumped from one steady state concentration of 0.2 μmol g^{-1} to another at 0.4 μmol g^{-1} on days 29 – 39.

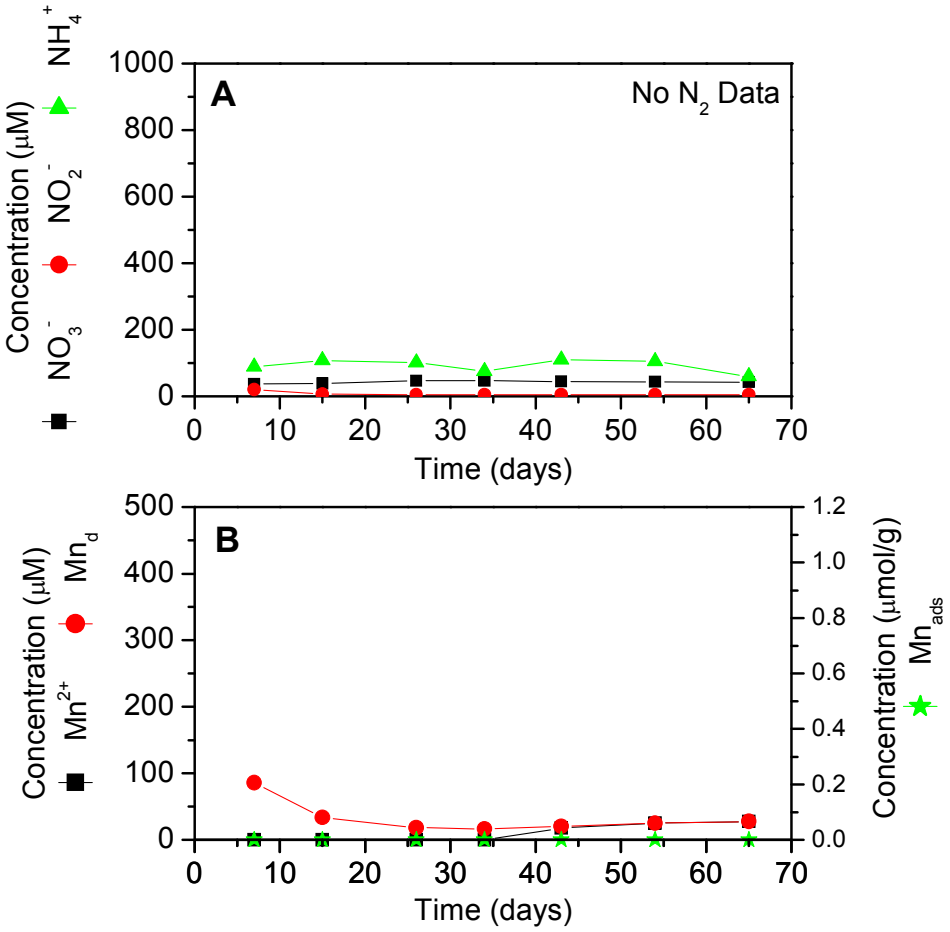

Figure 4.2: Time evolution for the deep sediment control incubation. (a) NH_4^+, NO_2^-, and NO_3^-. (b) Mn^{2+}, Mn_d, and Mn_{ads}. Mn_d was assumed to include $MnO_{2(c)}$ and Mn^{2+}. Mn_{ads} was assumed as adsorbed Mn^{2+}.

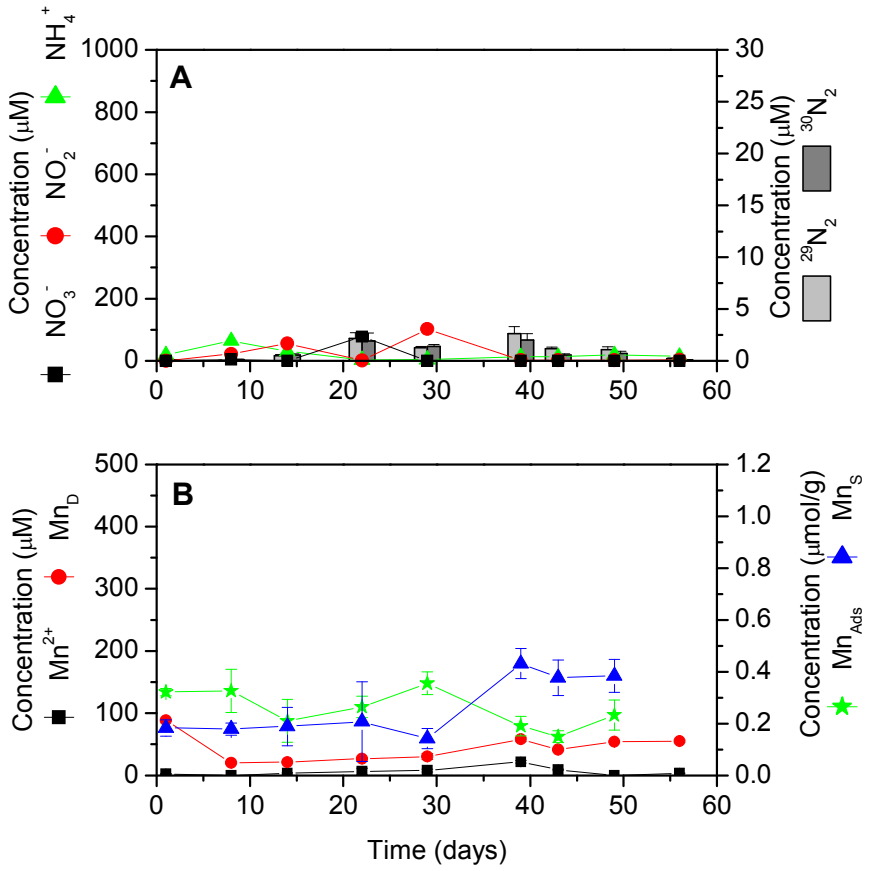

Figure 4.3: Time evolution for the shallow sediment control slurries. (a) NH_4^+, NO_2^-, NO_3^-, $^{29}N_2$, and $^{30}N_2$. (b) Mn^{2+}, Mn_d, Mn_{ads}, and Mn_s. Mn_d was assumed to include $MnO_{2(c)}$ and Mn^{2+}. Mn_{ads} was assumed as adsorbed Mn^{2+}. Mn_s includes only the reactive amorphous Mn-oxides.

4.2 Treatments containing $MnO_{2(c)}$ and NH_4^+

It was first necessary to determine the ideal ratio of N : Mn ratio that promotes Mn-catalyzed nitrification and/or denitrification in anaerobic conditions (Eq. 1.6 – 1.9). This objective was realized by varying the initial NH_4^+ : MnO_2 between 0.1:1 and 10:1 in separate sediment slurry incubations. Incubations were conducted for 80 days. Once steady state was reached, the percent of Mn^{2+} produced from the initial $MnO_{2(c)}$ was represented against the percent of the initial NH_4^+ removed (**Figure 4.4**). The data show that there is no apparent correlation between Mn^{2+} produced and NH_4^+ removed at low initial N : Mn ratios. In contrast, a strong correlation is found at initial N : Mn ratios greater than or equal to 2:1, suggesting that the production of Mn^{2+} may be linked to the consumption of NH_4^+ at higher nitrogen concentrations. According to our incubation at different NH_4^+ : $MnO_{2(c)}$ loads, the optimal N : Mn ratio range is between 2:1 and 10:1. The following incubations were therefore performed with an initial N : Mn ratio of 5:1 to ensure optimal conditions for Mn-catalyzed nitrification and/or denitrification.

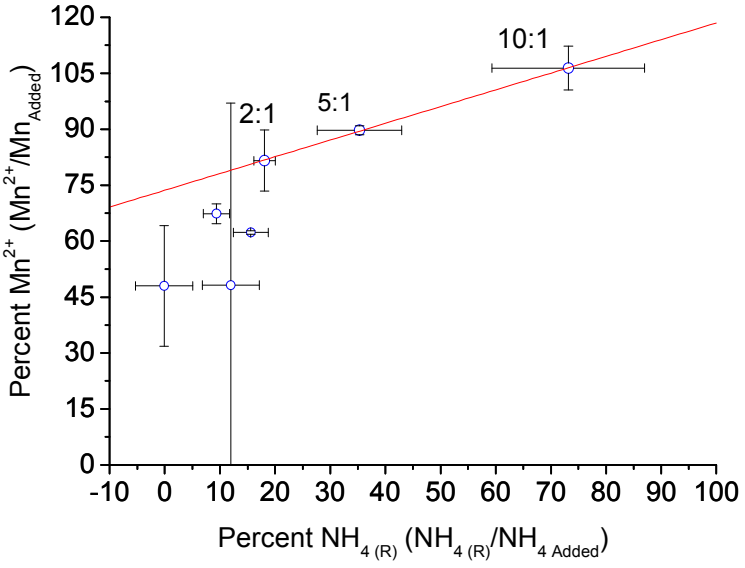

Figure 4.4: Percent of NH_4^+ removed ($NH_{4(R)}$) against percent of Mn^{2+} formed after 80 days in incubations conducted at increasing initial N : Mn ratios. Percents were needed since each treatment contained different initial concentrations of both $MnO_{2(c)}$ and NH_4^+. The ratios contained in the linear range are labeled.

Three other BTR incubations were conducted using 5:1 initial N:Mn ratios of isotope-labeled $^{15}NH_4^+$ and $MnO_{2(c)}$. The three slurry incubations were conducted with three different sediment sources and demonstrated the same general trends. **Figure 4.5** shows the results of the first of these incubations using shallow sediment. First, Mn_d reached a steady state of 80 μM after the initial decrease over 5 days. Mn^{2+} formation began slowly from day 10 to day 20 and reached a maximum around 70 μM at day 36. Mn_{ads} (under the form Mn^{2+}) increased at day 10 to a peak of 0.5 μmol g^{-1} at 30 days. This increase correlated with the rise to 60 μM ΣNO_x^- up to day 20. After 20 days, ΣNO_x^- decreased regularly to 10 μM at 36 days, then rebounded to 40 μM at 50 days. NH_4^+ initially increased in concentration to 1400 μM before dropping to 550 μM around the same time as Mn^{2+} formation. $^{29}N_2$ spiked at 25 μM around 30 days and correlated to the decrease in ΣNO_x^- concentration. $^{30}N_2$ also followed roughly the same trend with a peak of around 8 μM at 36 days.

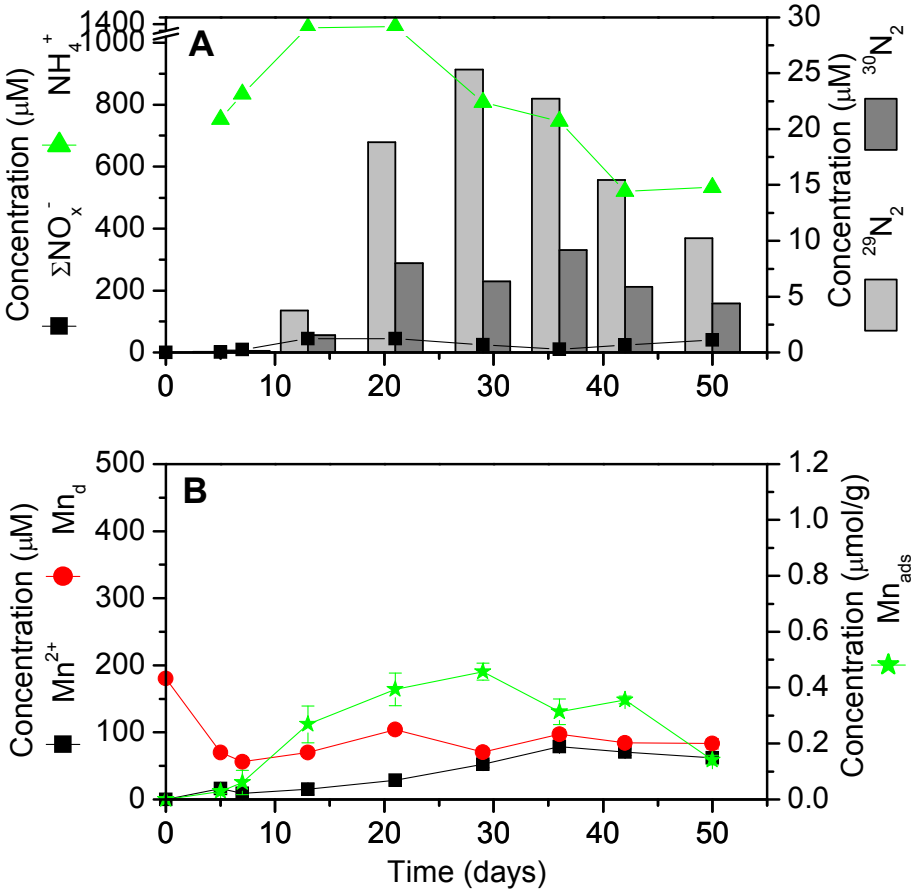

Figure 4.5: Time evolution of: (a) NH_4^+, fixed nitrogen (ΣNO_x^-), $^{29}N_2$, and $^{30}N_2$, and (b) Mn^{2+}, Mn_d, and Mn_{ads} in shallow sediment slurry incubations in the presence of 5:1 initial concentrations of $^{15}NH_4^+$: $MnO_{2(c)}$. Mn_d was assumed to include $MnO_{2(c)}$ and Mn^{2+}. Mn_{ads} was assumed as adsorbed Mn^{2+}.

Different results were found in the deeper sediment slurry incubation (**Figure 4.6**). Fixed nitrogen again increased around day 20, after BTR became anaerobic. This time, the NO_2^- and NO_3^- were measured separately. NO_2^- increased to 150 μM after 25 days before decreasing to a steady state value around 75 μM. NO_3^- was significantly lower than NO_2^-, with a maximum concentration of 40 μM. The NO_3^- initially decreased as the NO_2^- was formed then increased to the steady state maximum of 40 μM around 50 days. Only the last time step was measured for N_2. Both species concentrations were about the same with 19 μM of $^{29}N_2$ and 16 μM of $^{30}N_2$, but significantly above the control incubations (**Figure 4.2**)

The Mn data for this incubation produced different results than the previous incubation. First, no Mn_{ads} was ever detected during the incubation. Second, Mn_d remained roughly constant around 130 μM for the duration of the time series. Third, Mn^{2+} appeared initially, but dropped below detection limit by day 7. It eventually returned after day 34 and constituted all of Mn_d.

This second incubation was also the only incubation that generated dissolved sulfide during the course of the incubation. All three treatments from the same incubation contained a sulfide peak around the same time, and it decreased simultaneously with the increase in Mn^{2+} (**Figure 4.7**). Once dissolved sulfide was removed from solution, Mn^{2+} appeared in all the treatments.

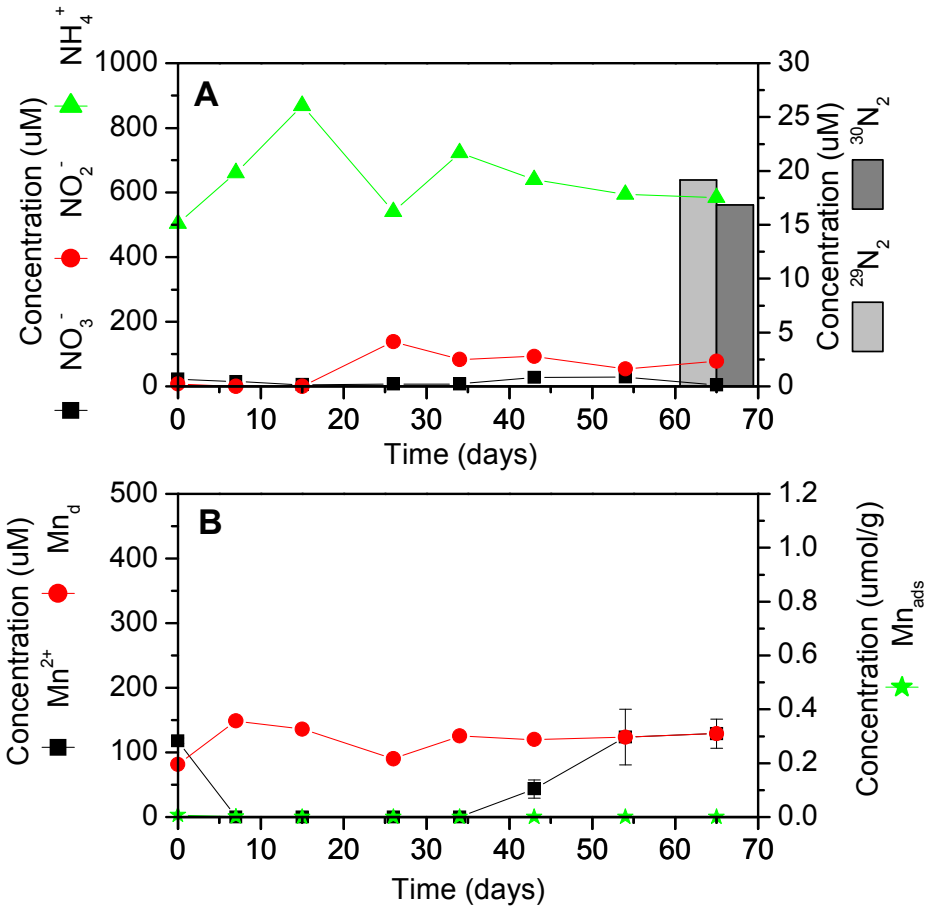

Figure 4.6: Time evolution of: (a) NH_4^+, NO_2^-, NO_3^-, $^{29}N_2$, and $^{30}N_2$, and (b) Mn^{2+}, Mn_d, and Mn_{ads} in deeper sediment slurry incubations in the presence of 5:1 initial concentrations of $^{15}NH_4^+$: $MnO_{2(c)}$. Mn_d was assumed to include $MnO_{2(c)}$ and Mn^{2+}. Mn_{ads} was assumed to include adsorbed Mn^{2+}.

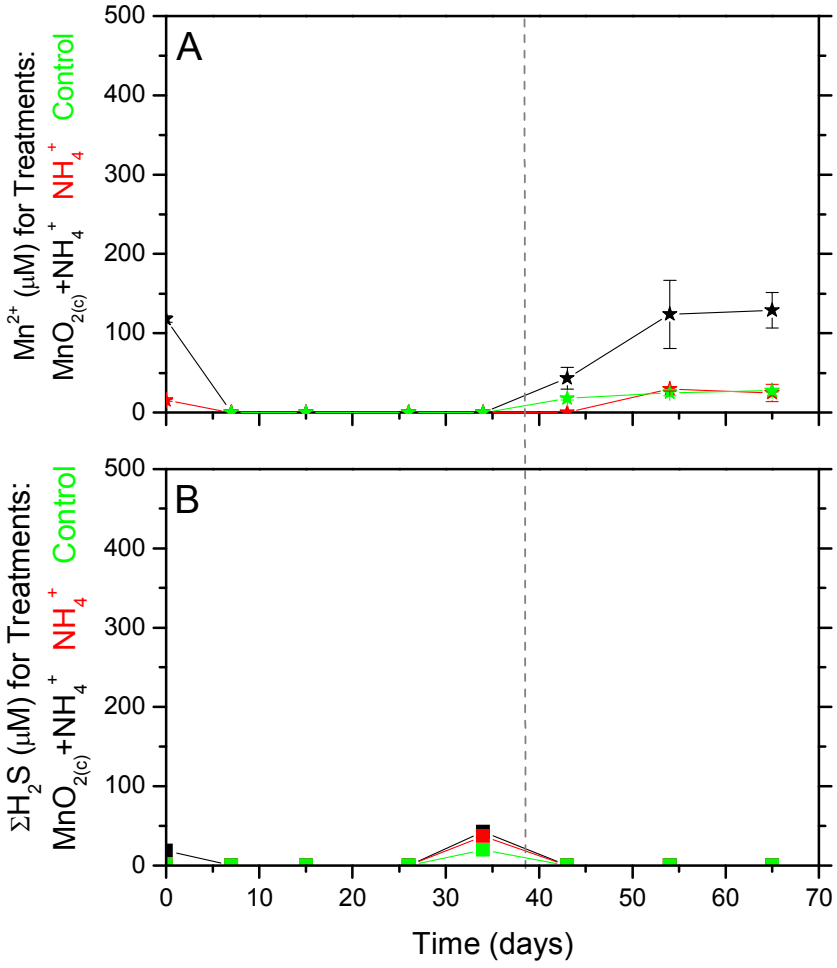

Figure 4.7: Time evolution for three treatments using the deeper (up to 15 cm) sediment. The stars represent Mn^{2+} (a) and the squares represent ΣH_2S (b) for the three treatments. The Mn^{2+} starts appearing in the reactors once the ΣH_2S decreases (vertical dotted line). The graphs are kept in the same scale for comparison.

The results from the last incubation (**Figure 4.8**) were similar to the first shallow sediment Mn-incubation discussed. The difference in the initial conditions was that $^{14}NO_3^-$ was also added to the sediment slurries, producing slightly higher maximum values in fixed nitrogen. NO_3^- increased initially to 100 μM at day 8, before it was removed from the system by day 22. NO_2^- increased from day 8 – 14 to a maximum of 200 μM before slowly decreasing to 140 μM by day 39. NO_2^- was finally removed from the system by day 39. NH_4^+ initially increased to 600 μM at day 8 before slowly decreasing to its steady state value around 200 μM. The two N_2 species stayed roughly the same concentrations initially, increasing to 20 μM on days 22 – 29 only. $^{29}N_2$ remained at steady state around 20 μM, while $^{30}N_2$ decreased to a steady state concentration of 12 μM by day 39. The Mn^{2+} data again correlated to the production of fixed nitrogen, with production from 8 – 14 days and an initial steady state concentration of 75 μM to day 39. Mn^{2+} then decreased from day 39 – 49 for a final steady state value of 50 μM. The Mn_d stayed fairly constant throughout the incubation at 150 μM. Mn_s showed a slow steady increase over the entire time series from 0.6 to 0.8 μmol g^{-1}. Mn_{ads} initially dropped from greater than 1.2 to 0.5 μmol g^{-1} over the first 14 days. It then peaked with the same general shape and timing as the Mn^{2+} with a maximum value of 0.7 μmol g^{-1} on day 22.

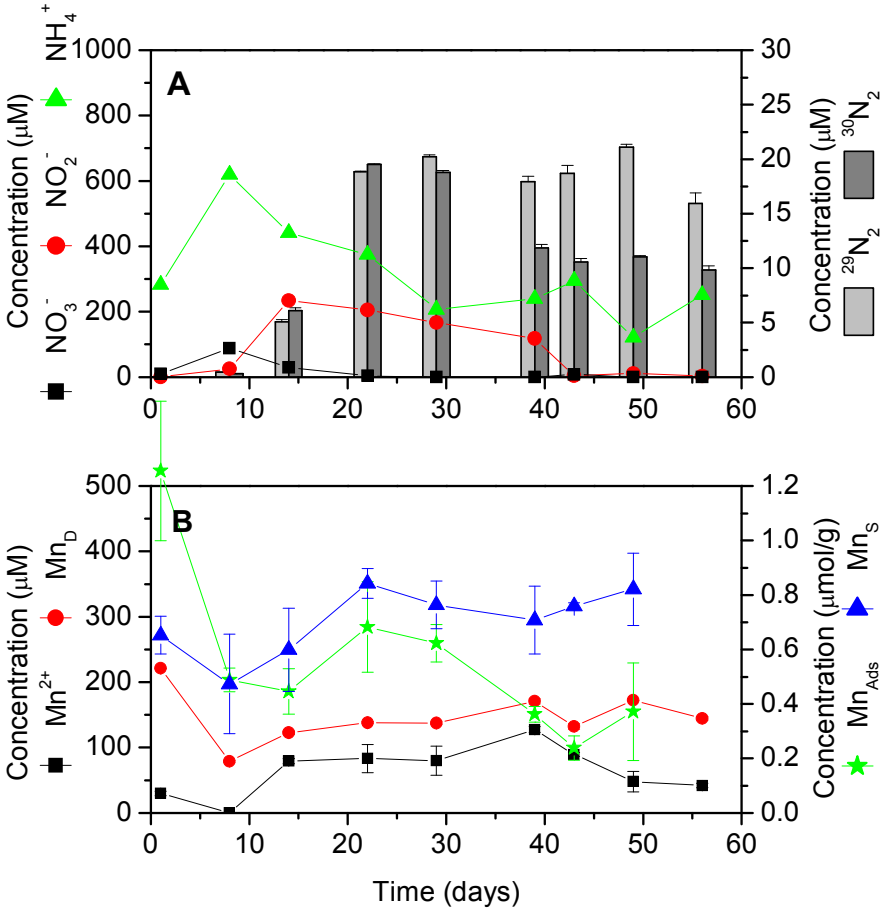

Figure 4.8: Time evolution for the $^{15}NH_4^+ + {}^{14}NO_3^- + MnO_{2(c)}$ treatment in shallow sediments. (a) NH_4^+, NO_2^-, NO_3^-, $^{29}N_2$, and $^{30}N_2$. (b) Mn^{2+}, Mn_d, Mn_{ads}, and Mn_s. Mn_d was assumed to include $MnO_{2(c)}$ and Mn^{2+}. Mn_{ads} represented adsorbed Mn^{2+} only. Mn_s included only the reactive amorphous Mn-oxides.

4.3 Treatments containing only $^{15}NH_4^+$

BTR incubations in the presence of isotope-labeled $^{15}NH_4^+$ but in the absence of $MnO_{2(c)}$ were also conducted in the two types of sediment to determine processes independent of the added Mn. The deeper sediment incubation without $MnO_{2(c)}$ (**Figure 4.9**) was similar to its counterpart incubation with $MnO_{2(c)}$ (**Figure 4.6**). NO_2^- and NO_3^- were produced after 15 days to steady state concentrations of 100 μM and 50 μM, respectively. NH_4^+ decreased dramatically to 200 μM at day 43 after its initial increase from 500 μM to 650 μM on day 15. NH_4^+ started increasing again to a final concentration of 350 μM. The final $^{29}N_2$ and $^{30}N_2$ concentrations were also roughly the same with values of 27 μM and 26 μM, respectively. The Mn speciation also shadowed the deep sediment $MnO_{2(c)}$ treatment with a steady state Mn_d concentration of 40 μM and Mn^{2+} production after 43 days. Again, Mn_d was entirely composed of Mn^{2+} at the end of the incubation.

The shallow sediment incubation without $MnO_{2(c)}$ (**Figure 4.10**) was also similar to its counterpart incubation with $MnO_{2(c)}$ (**Figure 4.8**). NH_4^+ increased initially from 400 μM to 600 μM in the first 8 days before decreasing to a steady state concentration of 250 μM at 39 days. NO_2^- increased slowly over 43 days to a maximum of 150 μM, and NO_3^- increased over the first 39 days to a maximum of 200 μM before it was removed from solution. Both $^{29}N_2$ and $^{30}N_2$ increased together for 22 days before decreasing to steady state at 39 days. $^{29}N_2$ increased to 16 μM before reaching a steady state of 11 μM, and $^{30}N_2$ increased to 23 μM before decreasing to an 8 μM steady state. In contrast to the incubations with $MnO_{2(c)}$ (**Figure 4.8**), Mn speciation appeared at steady state through the entire time series in this treatment (**Figure 4.10**). Mn_d stayed around 50 μM, Mn_{ads} changed only between 0.35 μmol g^{-1} and 0.5 μmol g^{-1}, and Mn_s varied between 0.2 μmol g^{-1} and 0.35 μmol g^{-1}. Mn^{2+} had a small production to 50 μM up to day 39 before disappearing by day 49.

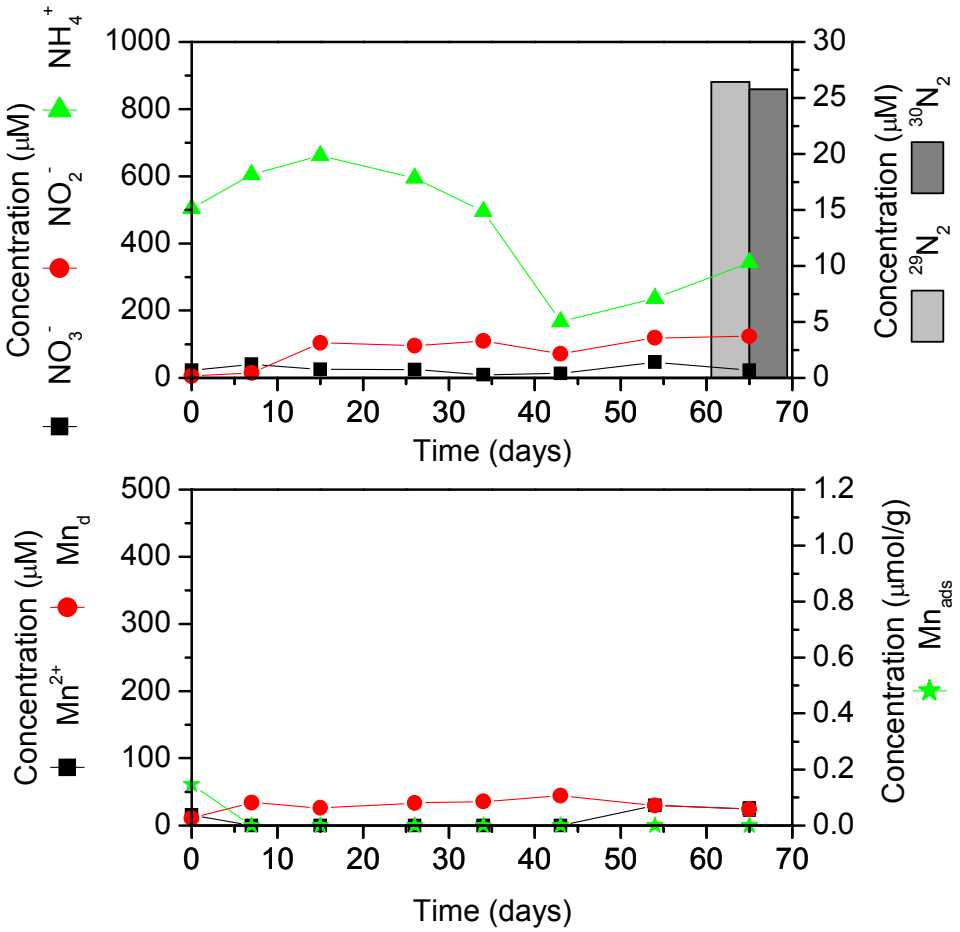

Figure 4.9: Time evolution for the $^{15}NH_4^+$-only treatment in the deeper sediment. (a) NH_4^+, NO_2^-, NO_3^-, $^{29}N_2$, and $^{30}N_2$, and (b) Mn^{2+}, Mn_d, and Mn_{ads}. Only the last time step of N_2 was analyzed. Mn_d was assumed to include $MnO_{2(c)}$ and Mn^{2+}. Mn_{ads} was assumed as adsorbed Mn^{2+}.

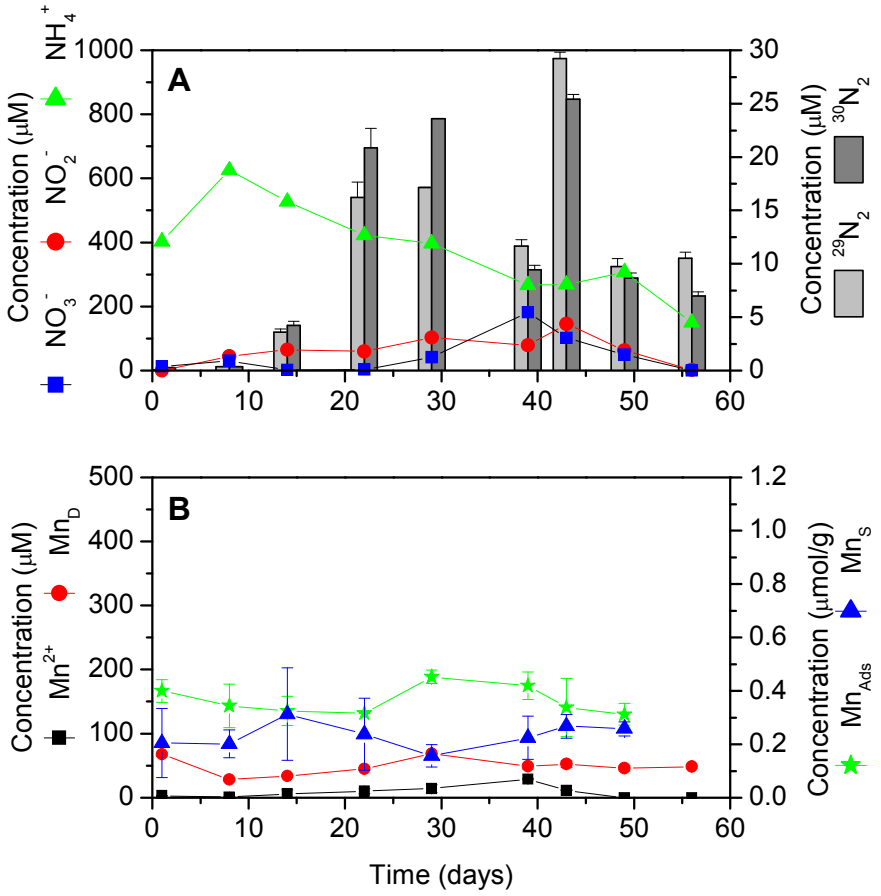

Figure 4.10: Time evolution for the shallower sediment $^{15}NH_4^+$-only treatment. : (a) NH_4^+, NO_2^-, NO_3^-, $^{29}N_2$, and $^{30}N_2$, and (b) Mn^{2+}, Mn_d, Mn_{ads}, and Mn_s. Mn_d was assumed to include $MnO_{2(c)}$ and Mn^{2+}. Mn_{ads} was assumed as adsorbed Mn^{2+}. Mn_s includes only the reactive amorphous Mn-oxides.

4.4 Testing for Heterotrophic Denitrification

One sediment slurry incubation – $MnO_{2(c)}$ + $^{14}NH_4^+$ + $^{15}NO_3^-$ – was conducted in the shallow sediment to test for the dominance of heterotrophic denitrification. While the dissolved species share similar trends with the other $MnO_{2(c)}$ treatments, the N_2 data was different (**Figure 4.11**). NH_4^+ initially increased from 300 μM to 600 μM over the first 8 days before decreasing to a steady state concentration of 350 μM at 14 days. NO_2^- increased to 250 μM at 14 days before being removed from the solution by day 39. NO_3^- peaked twice over the time series – 100 μM at 8 days, then a slower peak to 120 μM at 43 days. N_2 was insignificant in this treatment. $^{29}N_2$ was minimal with a broad peak of 5 μM at 39 days, ending the incubation at 2 μM. $^{30}N_2$ slowly increased from 2 μM to a maximum of 3.5 μM and dropped backed to a steady state value of 2 μM. The Mn speciation also followed the other $MnO_{2(c)}$ treatments. Mn^{2+} was produced over 14 days to a steady concentration of 75 μM, and dropped to a new steady state concentration of 40 μM between 39 and 49 days. Mn_d remained essentially the same around 130 μM during the course of the incubation; the concentration at day 43 may be an outlier. Mn_{ads} and Mn_s also remained steady at 0.5 μmol g^{-1} and 0.6 μmol g^{-1}, respectively.

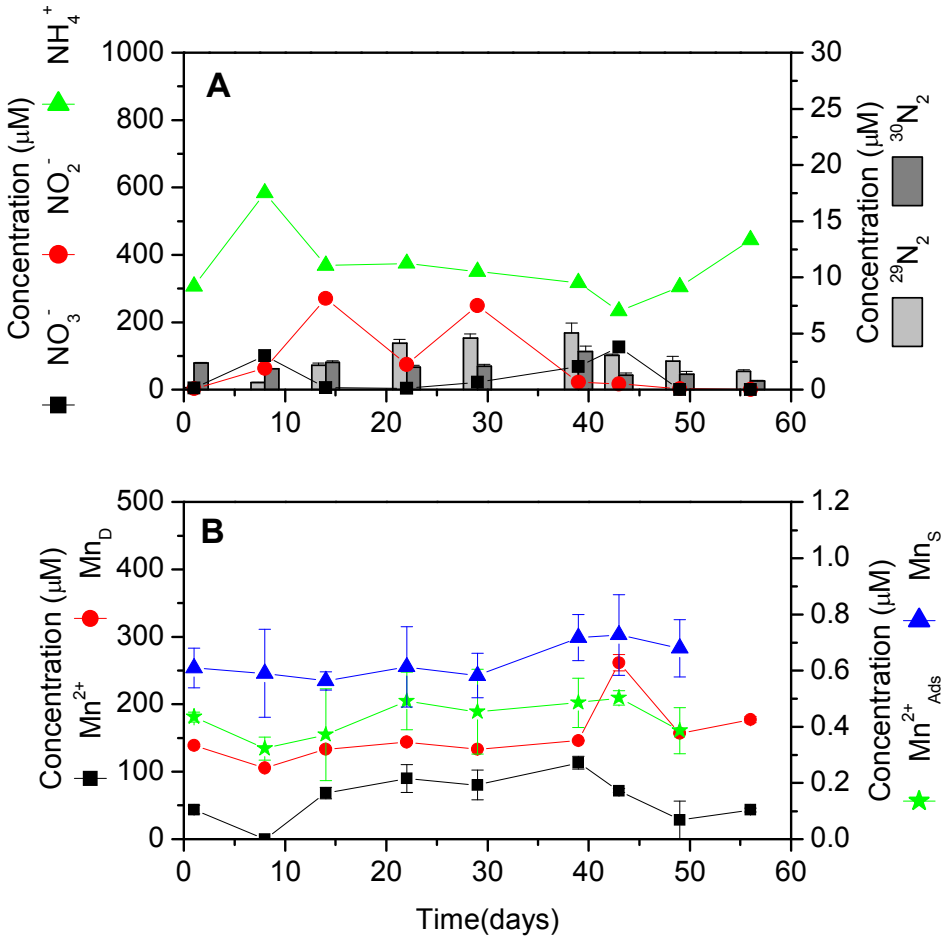

Figure 4.11: Time evolution for the shallower sediment $^{14}NH_4^+ + {}^{15}NO_3^- + MnO_{2(c)}$ treatment. (a) NH_4^+, NO_2^-, NO_3^-, $^{29}N_2$, and $^{30}N_2$. (b) Mn^{2+}, Mn_d, Mn_{ads}, and Mn_s. Mn_d was assumed to include $MnO_{2(c)}$ and Mn^{2+}. Mn_{ads} was assumed as adsorbed Mn^{2+}. Mn_s includes only the reactive amorphous Mn-oxides.

CHAPTER 5

DISCUSSION

A combination of depth microprofile measurements and sediment incubations were performed to determine possible nitrogen processes occurring in salt marsh sediments. The profile measurements were used as a guide to determine the sediment depth most suitable for the incubation studies by locating the areas of potential anaerobic nitrification. In this study, incubation experiments were used to define manganese influence on nitrogen cycling in anaerobic conditions.

The core taken in June 2004 shows fixed nitrogen concentrations well below the oxic zone (**Figure 4.1**). The classic understanding of nitrification requires oxygen to produce NO_2^- and NO_3^-. However, these two nitrogen components were detected in anaerobic sediments down to 80 mm. These data suggest either that O_2 penetrates the sediment deeper than previously thought (Neuhuber 2003) or that anaerobic nitrification is ongoing in salt marsh sediments. Anammox is known to occur at depth in all types of marine sediments (Jetten et al. 1999, Thamdrup and Dalsgaard 2002, Risgaard-Petersen et al. 2004, Vance-Harris and Ingall 2005), indicating a need for alternative NO_2^- and NO_3^- sources in anaerobic conditions. In this particular sediment, Mn^{2+} seems to be produced at two different depths: lower production between 0 and 20 mm and higher production between 20 and 30 mm. The production between 0 and 20 mm correlates to the first major peak in NO_2^- and NO_3^- (**Figure 4.1**). These data suggest that Mn may be involved in the nitrogen cycle as proposed by Luther et al. (1997).

Sediment slurry incubations were conducted to determine whether Mn is involved in nitrogen cycling. Batch tube reactors (BTR) are useful for incubating anaerobic sediments. BTR allow minimal gas diffusion through the glass, and rubber stoppers and aluminum caps minimize gas escape through the opening. BTR suffer from a few

disadvantages including a limited volume for analysis and the inability to change or refresh the added solution. To circumvent the volume limitations, multiple tubes were sacrificed for each incubation.

Control sediment slurries provided a background for Mn and N transformations in unperturbed sediments. The undisturbed shallow sediment and deeper sediment displayed roughly the same concentrations indicating that depth of sediment does not affect the natural release of NH_4^+ and Mn_d in sediment slurry incubations. On the other hand, fixed nitrogen background concentrations changed between shallow and deeper sediment. The deeper sediment incubation generated steady state concentrations of NO_3^-, and almost no NO_2^-, while the shallower sediment incubation generated various NO_2^- and NO_3^- concentrations over time. These data suggest that NO_2^- is removed at depth maybe through anammox and that the relative rate of production of NO_3^- exceeds denitrification rates at the surface.

5.1 Reproducibility of Incubations

Since BTR could not be sacrificed in triplicate at each time step of the incubations, the reproducibility of the incubations was tested by repeating incubations at least twice. Sediments are typically heterogeneous, but the replicate incubation sediment slurries produced the same general trends (**Figures 4.5** and **4.8**). This demonstrated that the processes occurring in this study are reproducible, not only within the individual sediment, but over multiple salt marsh sediment locations. The two shallow sediment $MnO_{2(c)}$-$^{15}NH_4^+$ incubations included sediment from a depth of 5-10 cm, and both resulted in nitrification and Mn reduction at the onset of NH_4^+ removal. For the shallow sediment incubations that included NO_3^- in the initial solution (**Figures 4.8** and **4.11**), the isotope-independent measurements (fixed nitrogen and Mn species concentrations) of the two $MnO_{2(c)}$ treatments ($^{15}NH_4^+ + {}^{14}NO_3^- + MnO_{2(c)}$ and $^{14}NH_4^+ + {}^{15}NO_3^- + MnO_{2(c)}$) produced almost identical results, again demonstrating reproducibility. Given the good

reproducibility of the results from these two incubations, the treatments without $MnO_{2(c)}$ and controls are also considered to produce reliable results.

5.2 Vertical Distribution of N Transformations and the Relation to Mn Reduction

As NH_4^+ concentrations are higher at depth, it is conceivable that Mn catalysis of the nitrogen cycle could occur in an area with a higher potential for anaerobic nitrification. Mortimer et al. (2004) found oxic nitrifying bacteria as deep as 40 cm, suggesting that the deeper sediment collected in this study could have potential for Mn catalysis. Interestingly, the sediment slurry incubation with deep sediments indicates that Mn catalysis is not as obvious in deeper sediments as it is in the shallower sediments (**Figures 4.7** and **4.8**). Mn^{2+} and Mn_{ads} were not detected in the deep sediment incubation pore waters until after 30 days, even though NO_2^- and NO_3^- were produced at the same time as NO_2^- and NO_3^- in the shallower sediment slurries. Either deeper anaerobic nitrification is unrelated to Mn reduction, or Mn-catalyzed nitrification does occur, but an outside pathway removes the Mn^{2+} before it is detected. The deeper sediment incubation was also the only incubation to display sulfide in the supernatant (**Figure 4.6**). Sulfide is known to precipitate readily with Fe^{2+} as FeS, and Mn^{2+} can adsorb onto the FeS surface (Huerta-Diaz et al. 1998) or coprecipitate with FeS (Arakaki and Morse 1993), possibly explaining the lack of Mn^{2+} in the dissolved phase until after sulfide was removed from the waters.

Deeper, salt marsh sediments are areas known for higher sulfide concentrations (e.g., Koretsky et al. 2003, Lowe et al. 2000). In a core taken in 2004 at the same location, sulfide was detected near the sediment –water interface (SWI) during rising tide (data not shown). In addition, Mn^{2+} was not detected at any depth, suggesting it was removed by adsorption or coprecipitation.

5.3 Evidence for Anaerobic Nitrification

Classic nitrification requires oxygen to form NO_2^- and NO_3^- (Bothe et al. 2000). Interestingly, the sediment profiles show NO_2^- and NO_3^- peaks 5 cm below the sediment-water interface (SWI). As stated above, either dissolved oxygen penetrates the sediment or anaerobic nitrification is taking place in these sediments.

One conclusion from Thamdrup and Dalsgaard (2000) was that their incubations might require different concentrations of NH_4^+ and MnO_2 than the experiments of Hulth et al. (1999) to find evidence for Mn-catalysis. The natural sediment of each site might require different initial compositions of substrate. A test incubation was first conducted to determine the optimal concentration ratio of NH_4^+ : $MnO_{2(c)}$ to find Mn-catalyzed nitrogen cycling. The concentrations used in the test incubation for initial N : Mn ratios were within concentrations measured in porewaters of similar sediment. Jahnke et al. (2003) found NH_4^+ concentrations between 0 and roughly 2500 μM in fresh and marine porewaters of the Satilla River, Georgia. Kostka et al. (2002) found concentrations around 500 μM NH_4^+ as well in the salt marsh at SkIO. The test incubation contained concentrations between 100 and 1000 μM NH_4^+. Anschutz et al. (2005) completed a complete Mn particulate study and found a maximum of roughly 50 μmol g^{-1} amorphous-MnO_2 in the top 10 cm of a marine sediment core. The highest concentration of colloidal manganese added in this study was 1000 μM which equates roughly to 2.5 μmol g^{-1} in BTR.

The test incubation measured ammonium removal over time. A maximum of roughly 75% of the ammonium initially added to the sediment was removed over the 80 days the incubation was run. Unfortunately, only Mn_d, Mn^{2+}, and NH_4^+ were measured, so the potential amount of NO_2^- and NO_3^- formed is unknown. The evidence for possible coupled anaerobic nitrification in the test incubation is the correlation with Mn^{2+} formed and NH_4^+ removed in specific reactor ratios. The best location to find a coupled reaction

is in the area of a linear correlation between species involved, or between 2:1 and 10:1 in this study (**Figure 4.4**).

In the presence of a 5:1 N : Mn ratio, the sediment slurry incubations demonstrated anaerobic NO_2^- and NO_3^- formation, indicating anaerobic nitrification in these salt marsh sediments. The appearance of NO_2^- and NO_3^- also correlates to Mn reduction. For both shallow sediment incubations (**Figure 4.4** and **4.7**), the NO_2^- and NO_3^- concentrations appear at the same time as Mn^{2+} and Mn_{ads}. Even though correlations do not automatically imply causality, the correlation between the two forms of Mn^{2+} and NO_2^- and NO_3^- formation seems to indicate Mn-coupled anaerobic nitrification in the first 20 days. Intuitively, the $MnO_{2(c)}$ treatments should accompany higher NO_2^- and NO_3^- formation than treatments without $MnO_{2(c)}$, and **Figure 5.1** verifies this assumption. The nitrogen concentrations measured in the $^{15}NH_4^+$-only treatment are subtracted from the nitrogen concentrations in the $^{15}NH_4^+$-$MnO_{2(c)}$ treatment of shallow sediment incubation results. The differences between the two treatments reveal which species are produced (positive values) or removed (negative values) at a higher rate in the presence of MnO_2 relative to the NH_4^+ only incubation. The treatments with $MnO_{2(c)}$ produced slightly higher concentrations of NO_3^- initially then produced significantly higher concentrations of NO_2^- until day 22. More NH_4^+ is also removed in the $MnO_{2(c)}$ treatments over the first 40 days. The higher NO_2^- and NO_3^- and lower NH_4^+ concentrations associated with the $MnO_{2(c)}$ treatment seem to indicate Mn is involved in the N cycle through catalyzed nitrification in the first 20 days.

Other than nitrification and anammox, NH_4^+ removal processes in salt marsh sediments include adsorption and biological uptake. Ammonium adsorption is affected by the organic matter content (Hou et al. 2003). Salt marsh sediments are rich in organic matter, indicating ammonium adsorption may be important in this study, but a 30 – 75% removal rate is unlikely due entirely to adsorption onto sediment slurries. Ammonium is also removed from solution by microbial uptake.

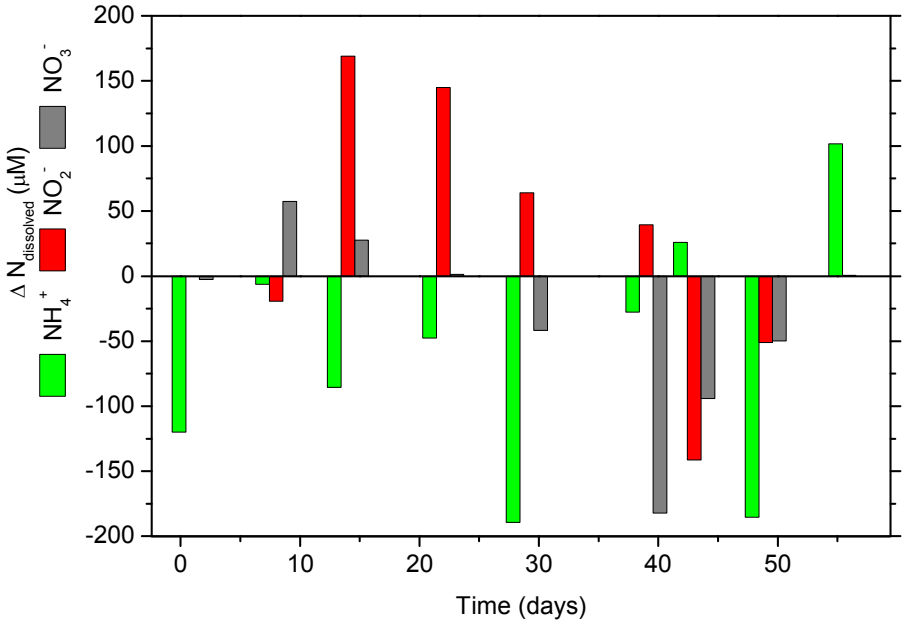

Figure 5.1: Change in concentrations between the $MnO_{2(c)}$ treatment and the treatment without $MnO_{2(c)}$ of the shallow sediment incubation shown in **Figure 4.8** and **4.10**. $\Delta N = N_{Mn} - N_{w/o\ Mn}$ where N_{Mn} is the concentration of each dissolved species from the $MnO_{2(c)}$ treatment and $N_{w/o\ Mn}$ is the concentration of each dissolved species from the treatment without $MnO_{2(c)}$. Positive values indicate higher production measurements, while negative values indicate higher removal measurements. Since the sediment slurries are reproducible in sediment from the same depths, this data is analogous to the other incubations from shallow sediments.

5.4 Denitrification in Salt Marsh Sediments

The most important and intriguing results from this study are the heterotrophic denitrification data. The $^{15}NO_3^-$ treatment showed $^{30}N_2$ produced at concentrations only slightly higher than control incubations, even over the entire 60 day incubation (**Figure 4.11**), indicating that heterotrophic denitrification and Mn-catalyzed denitrification through NO_3^- (Eq. 1.7) are not significant in these salt marsh sediments. Thus, heterotrophic denitrification should not play an important role in the other incubations as well. Assuming anaerobic nitrification is present in these sediments, $^{15}NH_4^+$-enriched incubations should oxidize $^{15}NH_4^+$ to $^{15}NO_2^-$ and $^{15}NO_3^-$. The fixed nitrogen of both isotopes (^{14}N and ^{15}N) would then produce $^{28}N_2$, $^{29}N_2$, and $^{30}N_2$ through the alternative denitrification pathways (Mn-catalyzed denitrification through NH_4^+ (Eq. 1.6) and anammox) discussed below.

Reduction of $MnO_{2(c)}$ coupled to NH_4^+ oxidation to N_2 (Eq. 1.6) is also found to not be a major pathway of N_2 production. The $MnO_{2(c)}$-$^{15}NH_4^+$ treatment (**Figure 4.8**) shows no detectable denitrification in the first 14 days. If direct NH_4^+ oxidation to N_2 coupled to $MnO_{2(c)}$ reduction was significant, $^{30}N_2$ would be detected in the beginning of the incubation. Two moles of $^{15}NH_4^+$ would oxidize to one mole of $^{30}N_2$. Therefore, Mn-catalyzed denitrification (Eq. 1.6 and 1.7) is not found in these salt marsh sediments. In turn, it is possible that Mn indirectly affects N_2 formation through the nitrification pathways discussed earlier (Eq. 1.8, 1.9, and 1.13). To determine the indirect effect of MnO_2, $^{29}N_2$ and $^{30}N_2$ concentrations from the $MnO_{2(c)}$-$^{15}NH_4^+$ shallow incubation were subtracted from the N_2 measurements of the $^{15}NH_4^+$ shallow incubation (**Figure 5.2**). $^{29}N_2$ is higher in concentration in the $MnO_{2(c)}$ treatment at all time steps, except for an outlier, while the time steps show a higher $^{30}N_2$ concentration in the $MnO_{2(c)}$ treatments after day 14 (**Figure 5.2**).

A potential explanation for increased denitrification in the $MnO_{2(c)}$ treatments is anammox. Anammox requires a NO_2^- or NO_3^- substrate (Eq. 1.3 – 1.4). Thus, a coupled

nitrification pathway that produces NO_2^- and NO_3^- must be present. The increased N_2 production in the $MnO_{2(c)}$ treatments after 14 days correlates to the increased production of NO_2^- and NO_3^- and the removal of NH_4^+ (**Figures 5.1** and **5.2**). $^{15}NH_4^+$ reacts directly with the $^{14}NO_3^-$ initially present in the incubations, producing $^{29}N_2$. $^{30}N_2$ forms through the reaction of $^{15}NH_4^+$ with the NO_2^- and NO_3^- produced through Mn-catalyzed nitrification of the $^{15}NH_4^+$. Since NH_4^+ appears in excess when compared to the total speciation of nitrogen in these sediments, the oxidation of NH_4^+ to NO_2^- and NO_3^- would not decrease the availability of NH_4^+ for anammox.

From the data, the following sequence of reactions in these incubations is proposed (**Figure 5.3**): *(1)* respiration consumes the O_2 initially present within the first couple of days; *(2)* MnO_2 oxidizes NH_4^+ to NO_2^- and NO_3^- through Mn-catalyzed anaerobic nitrification (Eq. 1.8 and 1.9) as indicated by increased production of NO_2^- and NO_3^- and decreases in NH_4^+ (**Figure 5.1**); *(3)* NO_2^- and/or NO_3^- produced in step 2 are combined with excess NH_4^+ to produce N_2 through anammox (Eq. 1.3 and 1.4) after 14 days (**Figure 5.2**). The different combinations of enriched nitrogen species initially included in the sediment slurries indicate that one denitrification process, anammox, dominates in these salt marsh sediments. As only a trace amount of N_2 (2 – 3 μM) is produced through heterotrophic denitrification (**Figure 4.11**) at the start of the incubation, the shallow sediment incubation measurements (**Figures 4.5**, **4.8**, and **4.10**) and treatment comparison data (**Figures 5.1** and **5.2**) indicate most N_2 is produced after 20 days. Denitrification must occur after anaerobic nitrification. These incubations lead to the conclusion that Mn-N coupling must exist in these sediments through Mn-catalyzed nitrification which, in turn, activates denitrification through anammox only.

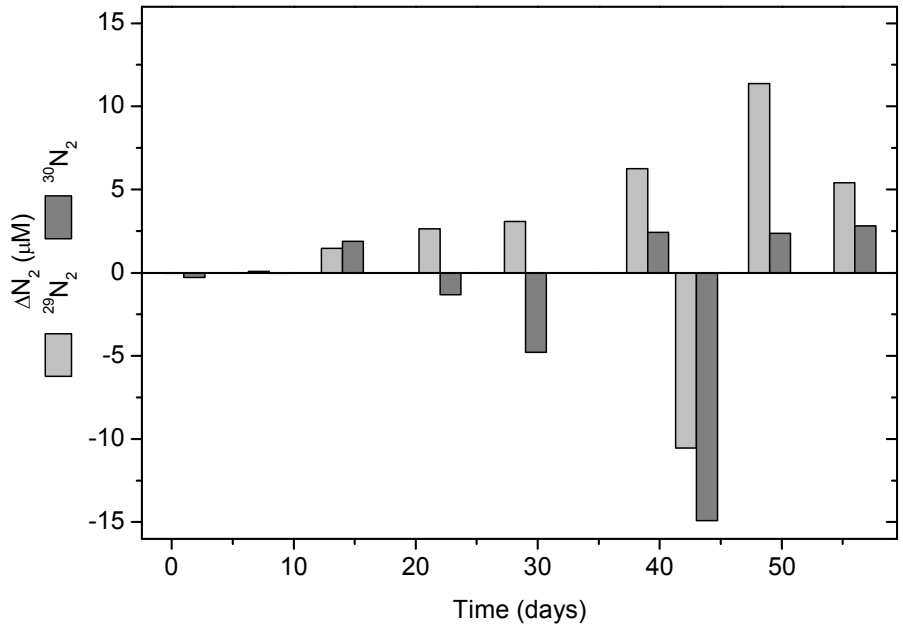

Figure 5.2: Change in concentrations between the $MnO_{2(c)}$ treatment and the treatment without $MnO_{2(c)}$ in one shallow sediment incubation. $\Delta N = N_{Mn} - N_{w/o\ Mn}$ where N_{Mn} is the concentration of each N_2 species from the $MnO_{2(c)}$ treatment and $N_{w/o\ Mn}$ is the concentration of each N_2 species from the treatment without $MnO_{2(c)}$. Since the sediment slurries indicate reproducibility between similar sediment, this data is analogous to the other incubations from shallow sediment.

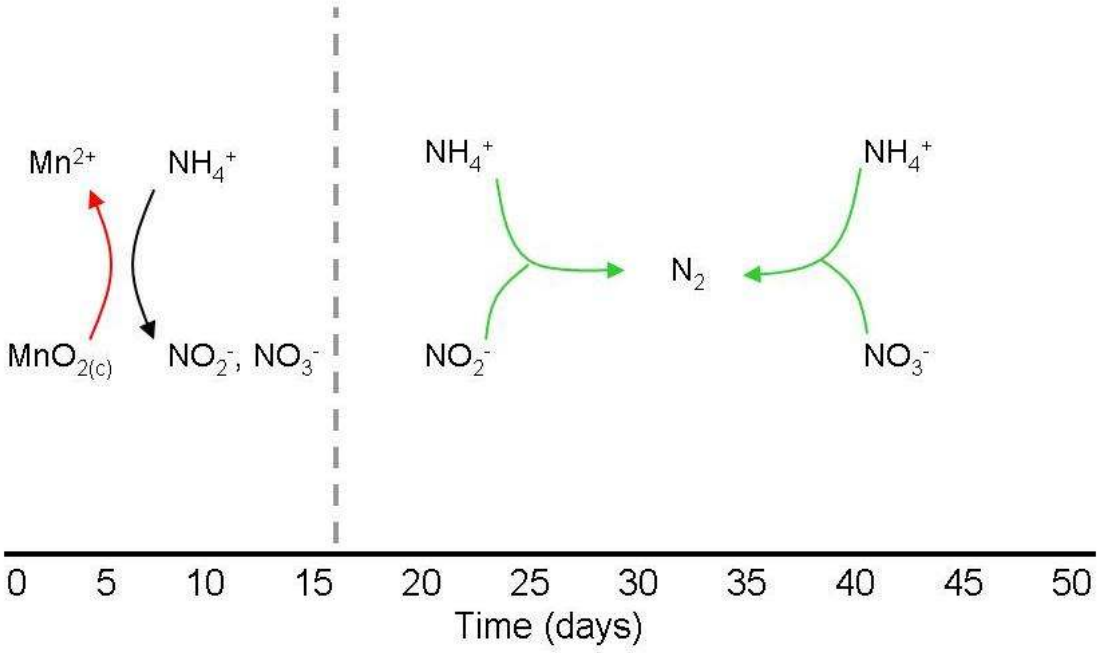

Figure 5.3: Schematic of the proposed processes occurring in shallow, anaerobic salt marsh sediments. For shallow sediment incubation slurries, manganese catalyzes nitrification anaerobically producing nitrate and nitrite. The nitrate and nitrite are then utilized as electron acceptors during anammox.

5.5 Anaerobic Nitrification and Denitrification rates in Salt Marsh Sediments

Initial nitrification rates were determined using the first 14 days (3 points per treatment) of the last incubation. The last incubation consisted of the most complete speciation obtained for both Mn and N in shallow salt marsh sediments (**Figure 4.8**, **4.10**, and **4.11**). A rate constant (k) was calculated assuming simple first-order kinetics with respect to each species and constant pH, organic matter, and dissolved inorganic carbon (DIC):

$$R_{nitrif} = \frac{d[NH_4^+]}{dt} = -k[NH_4^+][MnO_2] \quad (5.1)$$

Since the MnO_2 concentration was considered constant initially, the rate expression simplifies to a pseudo-first order rate law. The concentration of MnO_2 was combined with the rate constant to form a new observed rate constant. The initial nitrification rate was determined using the initial concentration of NH_4^+ (800 μM) and the calculated observed rate constant:

$$R_{nitrif} = k_{obs}[NH_4^+]_0 \quad (5.2)$$

The rates for the incubation are collected in **Table 5.1**. The nitrification rates are higher in the treatments containing an added $MnO_{2(c)}$, as expected for Mn-catalyzed anaerobic nitrification. Interestingly, the treatment with $^{14}NH_4^+$ and $MnO_{2(c)}$ displayed a faster rate than the treatment with $^{15}NH_4^+$ and $MnO_{2(c)}$. This could be evidence for possible biological fractionation of ^{15}N. The nitrifying organisms may oxidize $^{14}NH_4^+$ faster than $^{15}NH_4^+$. Nitrogen fractionation, preferential uptake of ^{14}N, has been found in denitrification pathways (Lehmann et al. 2004), suggesting that anammox organisms could also preferentially uptake $^{14}NH_4^+$. No information was found in the literature for nitrification.

Table 5.1: Pseudo first-order rate constants and nitrification rates for the different sediment slurry treatments. Rate constants (k_{obs}) are based on simple first-order kinetics. Nitrification rates represent the initial rate at the start of the incubations considering a $[NH_4^+]_0$ of 800 μM.

Treatment	k_{obs} (d^{-1})	Nitrification Rate (μM h^{-1})
$^{15}NH_4^+ + {}^{14}NO_3^-$	0.03 +/- 0.001	1.0
$^{15}NH_4^+ + {}^{14}NO_3^- + MnO_{2(c)}$	0.04 +/- 0.01	1.3
$^{14}NH_4^+ + {}^{15}NO_3^- + MnO_{2(c)}$	0.05 +/- 0.02	1.7

Heterotrophic denitrification rates between days 22 and 39 were determined using the same procedure and data from the $MnO_{2(c)}$-$^{14}NH_4^+$-$^{15}NO_3^-$ treatment. Again, we assumed simple first-order kinetics and excess organic carbon:

$$\frac{d[^{30}N_2]}{dt} = \frac{1}{2}k_{obs}[^{15}NO_3^-] = \frac{1}{2}k_{obs}([^{15}NO_3^-]_0 - [^{30}N_2]) \quad (5.3)$$

The concentration of NO_3^- for the initial heterotrophic denitrification rate calculation was the maximum concentration of 277 μM determined on day 14. Heterotrophic denitrification represents a small fraction of denitrification in these sediments with a rate of 0.007 μM h^{-1}.

Trimmer et al. (2003) conducted incubations with a 50/50 mixture of sediment and solution in their slurries to measure denitrification rates. They measured a heterotrophic denitrification rate of 110 nmol mL_{sed}^{-1} h^{-1} in incubated sediments from a marine estuary. Initial concentrations for their incubations required 18 mM $^{14}NH_4^+$ and 800 – 3200 μM $^{15}NO_2^-$ and/or $^{15}NO_3^-$. For the current study, 20 mL of slurry solution was added to 3 mL of sediment. This converts the heterotrophic denitrification rate (0.007 μM h^{-1}) to 0.87 nmol mL_{sed}^{-1} h^{-1}. The current study's incubations demonstrate a significantly lower heterotrophic denitrification rate (0.87 nmol mL_{sed}^{-1} h^{-1} compared to 110 nmol mL_{sed}^{-1} h^{-1}). Trimmer et al. (2003) measured significantly higher heterotrophic denitrification rates because the incubations started with NO_2^- and NO_3^- concentrations a

minimum of over ten times higher than in the current study. Since rates depend on the concentration of reactants, the higher concentration of NO_2^- and NO_3^- is responsible for the increased denitrification rate.

Anammox reaction rates were calculated using the $^{15}NH_4^+ + {}^{14}NO_3^-$ incubation instead of the treatment with $MnO_{2(c)}$ to minimize possible interference from Mn-catalysis. The anammox pathway combines one mole of $^{15}NH_4^+$ with one mole of $^{14}NO_x^-$ to form $^{29}N_2$. The rate was determined through the initial increase in $^{29}N_2$ since NH_4^+ and NO_3^- were present at the beginning of the incubation. Because two dependent species are involved in the kinetic rate, none of them in excess of the other, estimating the initial anammox rate becomes more complicated:

$$\frac{d[^{29}N_2]}{dt} = k[^{15}NH_4^+][^{14}NO_3^-] \qquad (5.4)$$

If the measured NH_4^+ is assumed to be completely enriched, $^{15}NH_4^+$ remains at a higher concentration than $^{14}NO_3^-$ (**Figure 4.10**) and is considered constant for the rate expression (Eq. 5.5). The rate then transforms into a simple pseudo-first order rate with dependence solely on $^{14}NO_3^-$. Unfortunately, the rate of anammox formation is not first-order with respect to NO_3^- using this assumption, making the rate expression too complicated to solve analytically. Therefore, the anammox rate was estimated using a linear approximation for $^{29}N_2$ production in the first 22 days (**Figure 5.4**). The anammox rate was measured at 0.05 $\mu M\ h^{-1}$.

Possible Mn influence on the rate of denitrification was determined by calculating the production rates of $^{29}N_2$ and $^{30}N_2$ for the $MnO_{2(c)}$-$^{15}NH_4^+$-$^{14}NO_3^-$ treatment and subtracting the same production rates from the $^{15}NH_4^+$-$^{14}NO_3^-$ treatment. Again, a simple linear approximation was needed to account for the complexity of the system. The difference between the two treatments represents the possible denitrification rate from Mn-catalysis. The $MnO_{2(c)}$-$^{15}NH_4^+$-$^{14}NO_3^-$ treatment produced N_2 (**Figure 5.2**) with denitrification rates of 0.06 $\mu M\ h^{-1}$ for both $^{29}N_2$ and $^{30}N_2$. This indicates that the $MnO_{2(c)}$

addition increased the rate of denitrification in $^{29}N_2$ between days 10 and 22 by 0.01 μM h^{-1}, a 17% increase, explaining the increased production of $^{29}N_2$ found in **Figure 5.2**. Conversely, $^{30}N_2$ was not affected by the $MnO_{2(c)}$ addition during the same period, with a 0.06 μM h^{-1} $^{30}N_2$ initial production rate for both treatments.

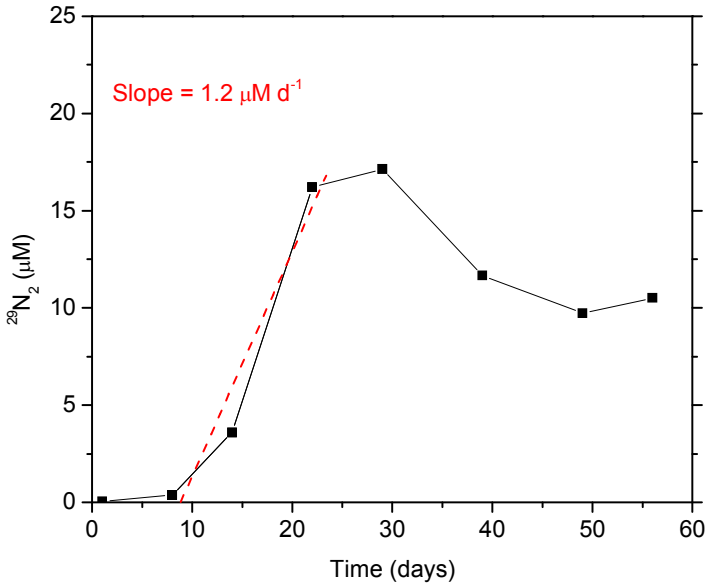

Figure 5.4: Rate of anammox based on the $^{15}NH_4^+ + {}^{14}NO_3^-$ sediment slurry incubations. The rate was calculated using the initial production of $^{29}N_2$.

In the first 20 days of the incubations, the presence of $MnO_{2(c)}$ should have had an effect on the denitrification rates of $^{30}N_2$. Even though both forms of Mn-catalyzed denitrification (Eq. 1.6 and 1.7) were not found to be substantial in salt marsh sediments, the Mn-catalyzed anaerobic nitrification pathway was significant over the first 20 days. **Figure 5.1** indicates that Mn affects production of NO_2^- and NO_3^- in the shallow sediment treatments containing $^{15}NH_4^+$. The increased production of NO_x^- should have increased the rates of denitrification through anammox with $^{15}NO_x^-$ (Eq. 1.3 and 1.4), thus enhancing the production of $^{30}N_2$. However, $^{14}NO_3^-$ was initially added to the incubations at a concentration of 50 μM. As the anammox organisms should

preferentially uptake the lighter $^{14}NO_x^-$, similar to heterotrophic denitrifiers (Lehmann et al. 2004), denitrification occurred preferentially through the $^{14}NO_x^-$ pathway (Eq. 1.3 and 1.4), increasing the production rate of $^{29}N_2$. As the initial anammox rates demonstrate, as long as $^{14}NO_x^-$ is present in the solution, the production rate of $^{29}N_2$ will be higher than the production rate of $^{30}N_2$ from biological fractionation.

Dalsgaard and Thamdrup (2002) measured anammox denitrification rates in incubations using 100 μM $^{14}NH_4^+$ and 50 μM $^{15}NO_3^-$. They calculated rates of 0.84 μM h^{-1} for $^{29}N_2$ production and 0.29 μM h^{-1} for $^{30}N_2$ production, both significantly higher than the rates found in the current study (0.05 μM h^{-1} and 0.06 μM h^{-1}, respectively) using $^{15}NH_4^+$ and $^{14}NO_3^-$. Dalsgaard and Thamdrup (2002) used full sediment incubations rather than slurry incubations, suggesting that higher anammox rates are due to the higher concentration of organisms in their incubations. Trimmer et al. (2003) also measured an anammox rate of 10 nmol mL_{sed}^{-1} h^{-1} with a 50/50 mixture of sediment and solution in their slurries as described above. For anammox incubations, initial concentrations included 18 mM $^{15}NH_4^+$ and 800 – 3200 μM $^{14}NO_2^-$ and/or $^{14}NO_3^-$. Using the same conversions discussed previously, the anammox rate of the current study was calculated as 14 nmol mL_{sed}^{-1} h^{-1}. The current study's incubations demonstrate a similar anammox rate (14 nmol mL_{sed}^{-1} h^{-1} compared to 10 nmol mL_{sed}^{-1} h^{-1}), because the incubation methods are more similar than in the Dalsgaard and Thamdrup (2002) study.

5.6 Modeling the Shallow Sediment Data to Further Prove the Existence of Mn-Catalysis

To provide supplementary proof for Mn-catalysis, a mathematical model was developed. The overall goal of this diagnostic model was to investigate whether Mn-catalyzed nitrogen cycling is possible by comparing the model results with the data. The system modeled was considered closed, so the initial concentrations of Mn and N added were used to balance the other species. $MnO_{2(c)}$ incubation data were found by subtracting the Mn^{2+} from Mn_d. Organic matter and H_2 gas were considered in abundance for simplicity in the rate expressions, and oxygen was absent. According to the sediment slurries, the pH never fluctuated more than 0.2, so pH was also constant in the model. These assumptions imply that the only change in the system is the form and concentrations of N and Mn species. No rate constants were found in the literature, therefore, all rate constants were optimized to fit the data. Isotopes of nitrogen species were included to follow the production of $^{29}N_2$ and $^{30}N_2$. Two simulations were conducted: one including the proposed Mn-coupling and one excluding the Mn-coupling. The Appendix describes the details of the diagnostic model including reactions, rate expressions, and rate constants.

The model, including the Mn-coupling, fit the data reasonably well (**Figure 5.5**). The model shows NH_4^+ decreasing during nitrification and N_2 formation during denitrification. NH_4^+ is removed as needed, when a rate expression for adsorption and biological uptake is considered. $^{29}N_2$ produced in the model depends on a high anammox rate through both NO_2^- (Eq. 1.3) and NO_3^- (Eq. 1.4). NO_2^- production in the model never reaches the concentrations measured in the incubations. The only source expressions for NO_2^- are from reduction of NO_3^- in the first step of heterotrophic denitrification (**Figure 1.1**) and oxidation of NH_4^+ by $MnO_{2(c)}$ (Eq. 1.13). The latter source is thermodynamically possible, yet speculative in natural sediments. Other processes that could produce nitrite in the incubations include the initial oxidation of NH_4^+ by O_2 to

NO_2^- (Eq. 1.1) and NO_3^- (Eq. 1.2), in the first few days after the beginning of the incubations. The data also show a higher NO_3^- concentration on day 8 than accounted for by the model (**Figure 5.5**). Oxygen was present at the beginning of the incubations, however, it is not considered in the model. Also, all reactions were considered pseudo first-order with respect to each species of interest. As discussed earlier, anammox does not fit pseudo first-order estimations with respect to NO_x^-. Therefore, some of the species in the model may also behave as second-order or third-order constituents in the kinetic expressions.

The Mn speciation from the model also demonstrates the correct trends and fits the data when the Mn-coupling is included. As the sediment is anaerobic, only one source of Mn oxidation is present in the model – Mn-catalyzed denitrification with NO_3^- (Eq. 1.7). The sediment used in the slurries also naturally contains a small amount of $MnO_{2(c)}$ and reactive amorphous MnO_2, but their release into solution is not accounted for in the model. The exclusion of background MnO_2 could also explain some of the deviation in the NO_2^- simulation, because the additional MnO_2 would be available for NH_4^+ oxidation to NO_2^- (Eq. 1.13).

The simulation excluding Mn-catalyzed nitrogen cycling demonstrates different results than the simulation with Mn-coupling (**Figure 5.5**). While the model is optimized to include Mn-catalysis, the simulation without Mn-coupling shows the importance of considering Mn- catalyzed nitrogen cycling. The simulation without Mn-coupling does not reduce MnO_2. In addition, only half of the NO_2^- is produced compared to the Mn-N simulation is produced. Since anaerobic nitrification is not allowed to occur, $^{30}N_2$ does not form. NH_4^+ and $^{29}N_2$ show little changes when the Mn-N coupling is not accounted for, since removal of NH_4^+ is dominated by uptake and adsorption and $^{29}N_2$ is produced through anammox – both independent of manganese reactions. If the model is optimized using the uncoupled simulation, Mn speciation could be reproduced by increasing the

heterotrophic Mn reduction rate. However, NO_2^- and $^{30}N_2$ would still show production rates unaccounted for without anaerobic Mn-catalyzed nitrification.

While the model does not directly verify the existence of Mn-catalysis, it produces output with the same general shapes as the measured data. Therefore, the Mn-catalyzed nitrogen cycling is again considered feasible in these sediments. From this model, Mn-catalyzed nitrification (Eq. 1.8, 1.9, and 1.13) accounts for all of the Mn reduction, and Mn-catalyzed denitrification (Eq. 1.6 and 1.7) is insignificant. Half of the formation of NO_2^- is through the first step of heterotrophic denitrification, while the other half is through NH_4^+ oxidation coupled with Mn reduction (Eq. 1.13), as seen through the two simulations (**Figure 5.5**). Nitrification, and subsequently $^{30}N_2$ production, is completely dependent on Mn-catalyzed nitrogen cycling. For denitrification, anammox is the predominant pathway accounting for all of the denitrification in the model. All other forms of denitrification are insignificant.

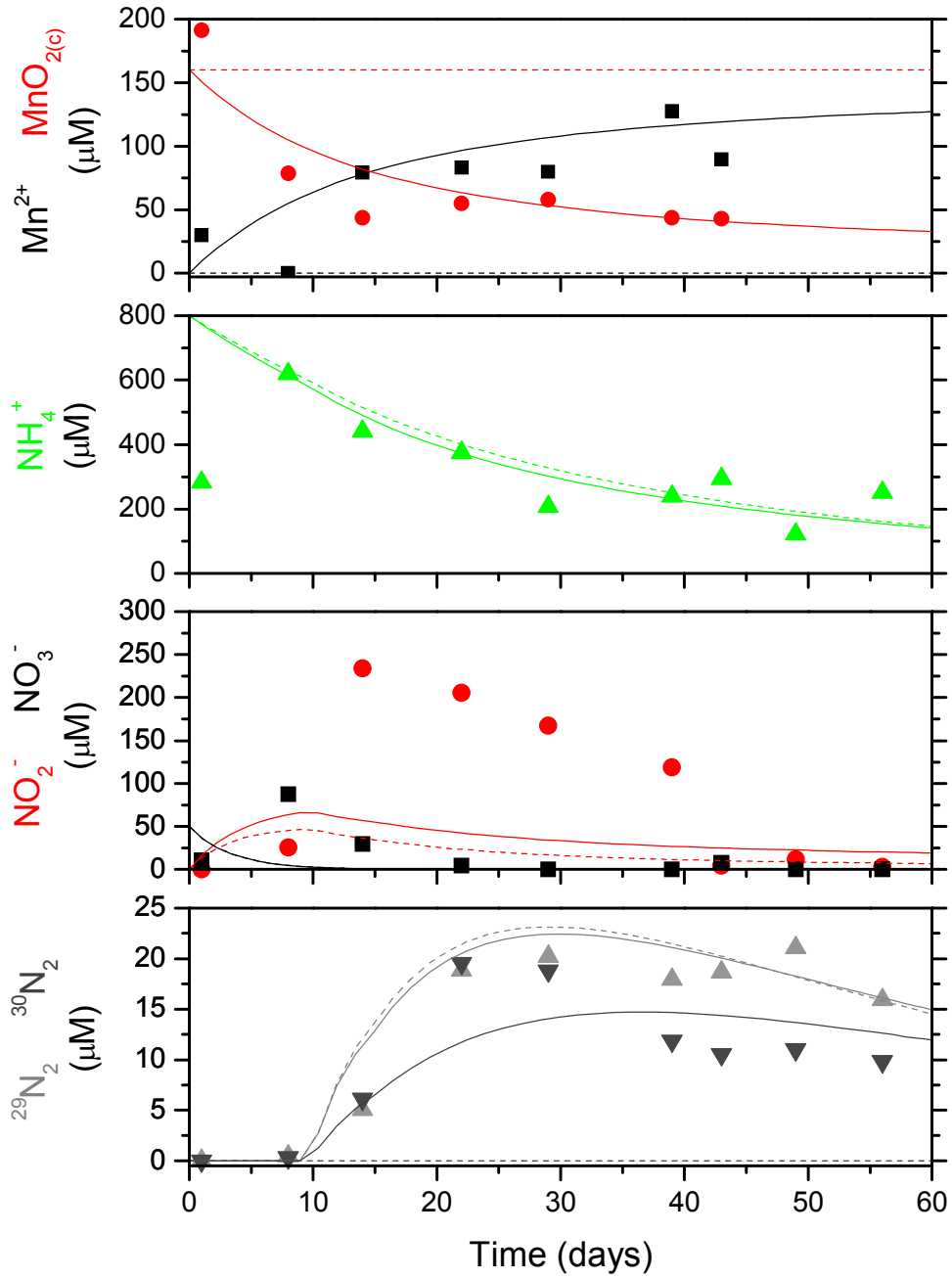

Figure 5.5: Output from the non-linear reaction model for the $^{15}NH_4^+ + {}^{14}NO_3^- + MnO_{2(c)}$ treatment. The data from the coupled model is labeled in solid lines, the uncoupled model in dashed lines, and actual incubation data by symbols. Colors match the colors from the incubation data (**Figure 4.8**).

CHAPTER 6

CONCLUSIONS

Nitrogen is an important nutrient in the global system. Therefore, the nitrogen cycle is essential to understand. Using the classic understanding of nitrogen cycling (Figure 1.1), the nitrogen budget is imbalanced with measured denitrification rates higher and fixed nitrogen concentrations lower than predicted. The imbalances may result from overlooking these potentially significant alternative pathways.

This study is only the second investigation to find proof of anaerobic nitrification. Hulth et al. (1999) also incubated marine sediments and found production of nitrate and nitrite in anaerobic treatments. While the initial conditions in the current study were different, both studies provide independent data indicating Mn-catalyzed nitrification. The only other incubation experiment conducted on anaerobic nitrification was Thamdrup and Dalsgaard (2000). Anoxic nitrification was not found in these sediments, though Mn reduction did occur. They stated that even though they did not find evidence for the anoxic nitrification, the process could be important in other environments. They also attributed the lack of evidence as compared to Hulth et al. (1999) to slight differences in concentrations of extractable Mn and NH_4^+. The current study accounted for these differences by running a test incubation to determine the optimal N : Mn ratio for NH_4^+ and $MnO_{2(c)}$. For salt marsh sediments, this ratio is between 2:1 and 10:1 (Figure 4.4).

The current study builds on the findings of Hulth et al. (1999) and Thamdrup and Dalsgaard (2000) to finally determine if anoxic nitrification is possible. This study followed Hulth et al. (1999) by adding an initial concentration of MnO_2 to initial concentrations of N species like in Thamdrup and Dalsgaard (2000). Through multiple incubation runs, NO_2^- and NO_3^- production was finally found in triplicate in anaerobic

salt marsh sediments, providing evidence for anaerobic nitrification. In the shallow sediment incubations, this anaerobic nitrification followed Mn reduction, demonstrating a possible pathway for NH_4^+ oxidation. It is the conclusion of this study that the potential for anaerobic nitrification does exist through NH_4^+ oxidation to NO_3^- and/or NO_2^- by MnO_2 reduction in salt marsh sediments.

The pathways of denitrification are more complicated. The classic N cycle uses a heterotrophic reduction pathway for denitrification from NO_3^- to NO_2^- and NO_2^- through a number of intermediate species to N_2. Each step in the chain requires a different reductase enzyme all found within denitrifying bacteria. Alternative pathways of anammox and Mn-catalysis include direct paths to N_2. Anammox requires NO_2^- or NO_3^- to oxidize NH_4^+ directly to N_2, while Mn-catalysis uses MnO_2 to oxidize NH_4^+ or Mn^{2+} to reduce NO_3^- for direct N_2 production.

This study found evidence that heterotrophic denitrification is not a substantial process in salt marsh sediments. Therefore, most of the N_2 produced in the incubations must be attributed to alternative pathways. High levels of $^{30}N_2$ and $^{29}N_2$ were found in the treatments without MnO_2, suggesting significant anammox rates. The MnO_2 treatments produced higher N_2 concentrations, implying that Mn is a catalyst for N_2 production. It is the conclusion of this study that Mn-catalyzed nitrification provides the NO_2^- and NO_3^- necessary for substantial N_2 production through anammox in anaerobic sediments.

To determine if these catalyzed reactions are occurring, pure culture experiments must be conducted on organisms similar to the ones catalogued by Mortimer et al. (2004). Pure culture incubations should include an inoculum of $^{15}NH_4^+$ and MnO_2. If Mn-catalyzed nitrification exists, the production of NO_2^- and NO_3^- will be apparent. Also, with these pure incubations, the kinetics of each reaction could be determined allowing the estimation of natural system rates. While the batch tube reactor (BTR) incubations

found evidence for Mn-catalyzed nitrification, more work is needed to understand fully the processes and reactions at work in the nitrogen cycle.

APPENDIX

CHARACTERIZATIONS OF THE DIAGNOSTIC MODEL

A diagnostic mathematical model was developed to provide supplementary proof for Mn-catalysis. A Runge-Kutta program was written using the ode45 function in Matlab. Equations in **Table A.1** were modeled with the initial conditions in the inoculum of the shallow sediment slurry incubation ($^{15}NH_4^+ + {}^{14}NO_3^- + MnO_{2(c)}$) of 800 μM $^{15}NH_4^+$, 50 μM $^{14}NO_3^-$, and 160 μM $MnO_{2(c)}$. All reaction rate expressions were developed assuming first-order kinetics with respect to each species (**Table A.2**). Organic matter, H_2, and pH were considered constant for simplicity. Therefore, the only species affecting the rates and changing in the system were the nitrogen and manganese species.

A phase lag of 10 days was placed on all denitrification rate components (**Table A.1** reactions (2), (4), (5), (7), and (8)) to simulate the denitrification delay from nitrification pathways. The two nitrogen isotopes, ^{14}N and ^{15}N, of each nitrogen species (NH_4^+, NO_2^-, and NO_3^-) as well as $^{29}N_2$ and $^{30}N_2$ were explicitly modeled. As a result, a total of ten different species, including manganese, were accounted for in the model. Nine non-linear differential equations were developed to include the nitrogen isotope dependence, and Mn^{2+} was determined through mass balance (**Table A.3**). Because NH_4^+ contained the sink through adsorption and biological uptake, no nitrogen species could be determined through mass balance. All reaction numbers from **Table A.1** carry through to **Tables A.2** and **A.3**.

Table A.1: Reaction network of the diagnostic mathematical model.

Heterotrophic denitrification

(1,2) $NO_3^- \xrightarrow{\text{nitrate reductase}} NO_2^- \xrightarrow{\text{multiple reductases}} N_2$

(3) $2CH_2O + NO_3^- + 2H^+ \rightarrow 2CO_2 + NH_4^+ + H_2O$

Anammox

(4) $5NH_4^+ + 3NO_3^- \rightarrow 4N_2 + 9H_2O + 2H^+$

(5) $NH_4^+ + NO_2^- \rightarrow N_2 + 2H_2O$

Heterotrophic Mn reduction

(6) $CH_2O + 2MnO_2 + 4H^+ \rightarrow 2Mn^{2+} + CO_2 + 3H_2O$

Mn-coupled denitrification

(7) $3MnO_2 + 2NH_4^+ + 4H^+ \rightarrow 3Mn^{2+} + N_2 + 6H_2O$

(8) $5Mn^{2+} + 2NO_3^- + 4H_2O \rightarrow 5MnO_2 + N_2 + 8H^+$

Mn-coupled nitrification

(9) $4MnO_2 + NH_4^+ + 6H^+ \rightarrow 4Mn^{2+} + NO_3^- + 5H_2O$

(10) $MnO_2 + NO_2^- + 2H^+ \rightarrow Mn^{2+} + NO_3^- + H_2O$

(11) $3MnO_2 + NH_4^+ + 4H^+ \rightarrow 3Mn^{2+} + NO_2^- + 4H_2O$???

Nitrogen fixation

(12) $N_2 \xrightarrow{H_2, CH_2O} 2NH_4^+$

Table A.2: Kinetic rate expressions for each reaction in Table A.1. All reactions assume first-order kinetics with respect to each species involved. Organic matter, H_2, and pH are absorbed into the k values.

$$R_1 = \frac{d[NO_2^-]}{dt} = -\frac{d[NO_3^-]}{dt} = k_1[NO_3^-]$$

$$R_2 = \frac{d[N_2]}{dt} = -\frac{1}{2}\frac{d[NO_2^-]}{dt} = k_2[NO_2^-]$$

$$R_3 = \frac{d[NH_4^+]}{dt} = -\frac{d[NO_3^-]}{dt} = k_3[NO_3^-]$$

$$R_4 = \frac{d[N_2]}{dt} = -\frac{4}{5}\frac{d[NH_4^+]}{dt} = -\frac{4}{3}\frac{d[NO_3^-]}{dt} = k_4[NH_4^+][NO_3^-]$$

$$R_5 = \frac{d[N_2]}{dt} = -\frac{d[NH_4^+]}{dt} = -\frac{d[NO_2^-]}{dt} = k_5[NH_4^+][NO_2^-]$$

$$R_6 = \frac{d[Mn^{2+}]}{dt} = -\frac{d[MnO_2]}{dt} = k_6[MnO_2]$$

$$R_7 = \frac{d[N_2]}{dt} = \frac{1}{3}\frac{d[Mn^{2+}]}{dt} = -\frac{1}{2}\frac{d[NH_4^+]}{dt} = -\frac{1}{3}\frac{d[MnO_2]}{dt} = k_7[MnO_2][NH_4^+]$$

$$R_8 = \frac{d[N_2]}{dt} = \frac{1}{5}\frac{d[MnO_2]}{dt} = -\frac{1}{2}\frac{d[NO_3^-]}{dt} = -\frac{1}{5}\frac{d[Mn^{2+}]}{dt} = k_8[Mn^{2+}][NO_3^-]$$

$$R_9 = \frac{d[NO_3^-]}{dt} = \frac{1}{4}\frac{d[Mn^{2+}]}{dt} = -\frac{d[NH_4^+]}{dt} = -\frac{1}{4}\frac{d[MnO_2]}{dt} = k_9[MnO_2][NH_4^+]$$

$$R_{10} = \frac{d[NO_3^-]}{dt} = \frac{d[Mn^{2+}]}{dt} = -\frac{d[NO_2^-]}{dt} = -\frac{d[MnO_2]}{dt} = k_{10}[MnO_2][NO_2^-]$$

$$R_{11} = \frac{d[NO_2^-]}{dt} = \frac{1}{3}\frac{d[Mn^{2+}]}{dt} = -\frac{d[NH_4^+]}{dt} = -\frac{1}{3}\frac{d[MnO_2]}{dt} = k_{11}[MnO_2][NH_4^+]$$

$$R_{12} = \frac{1}{2}\frac{d[NH_4^+]}{dt} = -\frac{d[N_2]}{dt} = k_{12}[N_2]$$

Table A.3: Combined reaction rate expressions. Separate expressions were used to differentiate between the nitrogen isotopes. Uptake/adsorption was a sink term included to represent biological uptake of NH_4^+ and adsorption of NH_4^+ onto sediment surfaces. Mn^{2+} was determined by mass balance.

$$\frac{d[^{15}NH_4^+]}{dt} = k_3[^{15}NO_3^-] + 2k_{12}[^{30}N_2] + k_{12}[^{29}N_2] - \frac{5}{4}k_4[^{15}NH_4^+][^{14}NO_3^-] - \frac{5}{4}k_4[^{15}NH_4^+][^{15}NO_3^-] - k_5[^{15}NH_4^+][^{14}NO_2^-] - k_5[^{15}NH_4^+][^{15}NO_2^-] - 2k_7[MnO_2][^{15}NH_4^+]$$
$$- k_9[MnO_2][^{15}NH_4^+] - k_{11}[MnO_2][^{15}NH_4^+] - \text{uptake / adsorption}$$

$$\frac{d[^{14}NH_4^+]}{dt} = k_3[^{14}NO_3^-] + k_{12}[^{29}N_2] - \frac{5}{4}k_4[^{14}NH_4^+][^{14}NO_3^-] - \frac{5}{4}k_4[^{14}NH_4^+][^{15}NO_3^-] - k_5[^{14}NH_4^+][^{14}NO_2^-] - k_5[^{14}NH_4^+][^{15}NO_2^-] - 2k_7[MnO_2][^{14}NH_4^+]$$
$$- k_9[MnO_2][^{14}NH_4^+] - k_{11}[MnO_2][^{14}NH_4^+] - \text{uptake / adsoption}$$

$$\frac{d[^{15}NO_2^-]}{dt} = k_1[^{15}NO_3^-] + k_{11}[MnO_2][^{15}NH_4^+] - k_5[^{15}NH_4^+][^{15}NO_2^-] - k_5[^{14}NH_4^+][^{15}NO_2^-] - k_{10}[MnO_2][^{15}NO_2^-] - 2k_2[^{15}NO_2^-]$$

$$\frac{d[^{14}NO_2^-]}{dt} = k_1[^{14}NO_3^-] + k_{11}[MnO_2][^{14}NH_4^+] - k_5[^{15}NH_4^+][^{14}NO_2^-] - k_5[^{14}NH_4^+][^{14}NO_2^-] - k_{10}[MnO_2][^{14}NO_2^-] - 2k_2[^{14}NO_2^-]$$

$$\frac{d[^{15}NO_3^-]}{dt} = k_9[MnO_2][^{15}NH_4^+] + k_{10}[MnO_2][^{15}NO_2^-] - k_1[^{15}NO_3^-] - k_3[^{15}NO_3^-] - \frac{3}{4}k_4[^{15}NH_4^+][^{15}NO_3^-] - \frac{3}{4}k_4[^{14}NH_4^+][^{15}NO_3^-] - 2k_8(Mn_T - [MnO_2])[^{15}NO_3^-]$$

$$\frac{d[^{14}NO_3^-]}{dt} = k_9[MnO_2][^{14}NH_4^+] + k_{10}[MnO_2][^{14}NO_2^-] - k_1[^{14}NO_3^-] - k_3[^{14}NO_3^-] - \frac{3}{4}k_4[^{15}NH_4^+][^{14}NO_3^-] - \frac{3}{4}k_4[^{14}NH_4^+][^{14}NO_3^-] - 2k_8(Mn_T - [MnO_2])[^{14}NO_3^-]$$

$$\frac{d[^{29}N_2]}{dt} = k_2([^{15}NO_2^-][^{14}NO_2^-])^{1/2} + k_7[MnO_2]([^{15}NH_4^+][^{14}NH_4^+])^{1/2} + k_8(Mn_T - [MnO_2])([^{15}NO_3^-][^{14}NO_3^-])^{1/2} + k_4[^{15}NH_4^+][^{14}NO_3^-] + k_4[^{14}NH_4^+][^{15}NO_3^-]$$
$$+ k_5[^{15}NH_4^+][^{14}NO_2^-] + k_5[^{14}NH_4^+][^{15}NO_2^-] - k_{12}[^{29}N_2]$$

$$\frac{d[^{30}N_2]}{dt} = k_2[^{15}NO_2^-] + k_7[MnO_2][^{15}NH_4^+] + k_8(Mn_T - [MnO_2])[^{15}NO_3^-] + k_4[^{15}NH_4^+][^{15}NO_3^-] + k_5[^{15}NH_4^+][^{15}NO_2^-] - k_{12}[^{30}N_2]$$

$$\frac{d[MnO_2]}{dt} = 5k_8(Mn_T - [MnO_2])[NO_3^-] - k_6[MnO_2] - 3k_7[MnO_2][NH_4^+] - 4k_9[MnO_2][NH_4^+] - k_{10}[MnO_2][NO_2^-] - 3k_{11}[MnO_2][NH_4^+]$$

$$[Mn^{2+}] = Mn_T - [MnO_2]$$

REFERENCES

Aller, R.C., J.E. Mackin (1989). "Open-incubation, diffusion methods for measuring solute reaction rates in sediments." **Journal of Marine Research (47)**: 411-440.

Anschultz, P. A., B. Sundby, L. Lefrancois, G.W. Luther III, A. Mucci (2000). "Interactions between metal oxides and species of nitrogen and iodine in bioturbated marine sediments." **Geochimica et Cosmochimica Acta (64)**: 2751-2763.

Anschutz, P., K. Dedieu, F. Desmazes, and G. Chaillou (2005). "Speciation, oxidation state, and reactivity of particulate manganese in marine sediments." **Chemical Geology (218)**: 265-279.

Arakaki, T. and J.W. Morse (1993). "Coprecipitation and adsorption of Mn(II) with mackinawite (FeS) under conditions similar to those found in anoxic sediments." **Geochimica et Cosmochimica Acta (57)**: 9-14.

Bothe, H., G. Jost, M. Schloter, B.B. Ward, and K.P. Witzel (2000). "Molecular analysis of ammonia oxidation and denitrification in natural environments." **FEMS Microbiology Reviews (24)**: 673-690.

Brendel, P. J., G.W. Luther III (1995). "Development of a gold amalgam voltammetric microelectrode for the determination of dissolved Fe, Mn, O2, and S(-II) in porewaters of marine and freshwater sediments." **Environmental Science and Technology (29)**: 751-761.

Bull D.C., M. Taillefert (2001). "Seasonal and topographic variations in porewaters of a southeastern USA salt marsh as revealed by voltammetric profiling." **Geochemical Transactions (13)**: 104-111.

Dalsgaard, T., D.E. Canfield, J. Petersen, B. Thamdrup, J. Acuna-Gonzalez (2003). "N2 production by the annamox reaction in the anoxic water column of Golfo Dulce, Costa Rica." **Nature (422)**: 606-608.

Dalsgaard, T. and B. Thamdrup (2002). "Factors controlling anaerobic ammonium oxidation with nitrite in marine sediments." **Applied and Enviornmental Microbiology (68)**: 3802-3808.

Deflandre, B., A. Mucci, J.P. Gagne, C. Guignard, B. Sundby (2002). "Early Diagenetic processes in coastal marine sediments disturbed by a catastrophic sedimentation event." **Geochimica et Cosmochimica Acta (66)**: 2547-2558.

Devol, A.H., L.A. Codispoti, J.P. Christensen (1997). "Summer and winter denitrification rates in western Arctic shelf sediments." **Continental Shelf Research (17)**: 1029-1050.

Dickson, A.G. (1993). "Thermodynamics of the dissociation of boric acid in synthetic sea water from 273.15 to 318.15 K." **Deep-Sea Reasearch (37)**: 755-766.

Froelich, P.N., G.P. Klinkhammer, M.L. Bender, N.A. Luedtke, G.R. Heath, D. Cullen, and D. Dauphin (1979). "Early oxidation of organic matter in pelagic sediments of the Eastern Equatorial Atlantic: Suboxic diagenesis." **Geochimica et Cosmochimica Acta (43)**: 1075-1090.

Hou, L.J., M. Liu, H.Y. Jiang, S.Y. Xu, D.N. Ou, Q.M. Liu, and B.L. Zhang (2003). "Ammonium adsorption by tidal flat surface sediments from the Yangtze estuary." **Environmental Geology (45)**: 72-78.

Huerta-Diaz, M.A., A. Tessier, and R. Carignan (1998). "Geochemistry of trace metals associated with reduced sulfur in freshwater sediments." **Applied Geochemistry (13)**: 213-233.

Hulth, S., R.C. Aller, and F. Gilbert (1999). "Coupled anoxic nitrification/manganese reduction in marine sediments." **Geochimica et Cosmochimica Acta (63)**: 49-66.

Jahnke, R. A., C.R. Alexander, and J.E. Kostka (2003). "Advective pore water input of nutrients to the Satilla River Estuary, Georgia, USA." Estuarine Coastal and Shelf Science **56**: 641-653.

Jetten, M. S. M., M. Strous, K.T. van de Pas-Schoonen, J. Schalk, U.G.J.M. van Dongen, A.A. van de Graaf, S. Logemann, G. Muyzer, M.C.M. van Loosdrecht, and J.G. Kuenen (1999). "The anaerobic oxidation of ammonium." **FEMS Microbiology Reviews** (**22)**: 421-437.

Jones, M.L., S.K. Liehr, J.J. Classen, W. Robarge (2000). "Mechanisms of dinitrogen gas formation in anaerobic lagoons." **Advances in Environmental Research (4)**: 133-139.

Kana, T.M., C. Darkangelo, M.D. Hunt, J.B. Oldham, G.E. Bennett, and J.C. Cornwell (1994). "Membrane inlet mass spectrometer for rapid high-precision determination of N_2, O_2, and Ar in environmental water samples." **Analytical Chemistry (66)**: 4166-4170.

Kana, T. M., M.B. Sullivan, J.C. Cornwell, and K.M. Groszkowski (1998). "Denitrification in estuarine sediments determined by membrane inlet mass spectrometry." **Limnology and Oceanography (43)**: 334-339.

Koretsky, C.M., C.M. Moore, K.L. Lowe, C. Meile, T.J. DiChristina, and P. Van Cappellen (2003). "Seasonal oscillation of microbial iron and sulfate reduction in saltmarsh sediments (Sapelo Island, GA, USA)." **Biogeochemistry (64)**: 179-203.

Kostka, J.E., B. Gribsholt, E. Petrie, D. Dalton, H. Skelton, and E. Kristensen (2002). "The rates and pathways of carbon oxidation in bioturbated saltmarsh sediments." **Limnology and oceanography (47)**: 230-240.

Kuypers, M. M. M., A.O. Sliekers, G. Lavik, M. Schmid, B.B. Jørgensen, J.G. Kuenen, J.S.S. Damste, M. Strous, and M.S.M. Jetten (2003). "Anaerobic ammonium oxidation in the Black Sea." **Nature (422)**: 608-611.

Lehmann, M.F., D.M. Sigman, and W.M. Berelson (2004). "Coupling the $^{15}N/^{14}N$ and $^{18}O/^{16}O$ of nitrate as a constraint on benthic nitrogen cycling." **Marine Chemistry (88)**: 1-20.

Lowe, K.L., T.J. DiChristina, A.N. Roychoudhury, and P. Van Cappellen (2000). "Microbiological and geochemical characterization of microbial Fe(III) reduction in salt marsh sediments." **Geomicrobiology Journal (17)**: 163-178.

Luther III, G. W., J.I. Popp (2002). "Kinetics of the abiotic reduction of polymeric manganese dioxide by nitrite: An anaerobic nitrification reaction." **Aquatic Geochemistry (8)**: 15-36.

Luther III, G. W., B. Sundby, B.L. Lewis, P.J. Brendel, and N. Silverberg (1997). "Interactions of manganese with the nitrogen cycle: Alternative pathways to dinitrogen." **Geochimica et Cosmochimica Acta (61)**: 4043-4052.

Madigan, M.T., J.M. Martinko, J. Parker (2003). **Brock Biology of Microorganisms**. Pearson Education Inc., Upper Saddle River, NJ.

Martens, C.S., R.A. Berner (1974). "Methane production in the interstitial waters of sulfate-depleted marine sediments." **Science (185)**: 1167-1169.

Middelburg, J.J., K. Soetaert, P.M.J. Herman, C.H.R. Heip (1996). "Denitrification in marine sediments: A model study." **Global Biogeochemical Cycles (10)**: 661-673.

Mohan, S.B., M. Schmid, M. Jetten, J. Cole (2004). "Detection and widespread distribution of the nrfA gene encoding nitrite reduction to ammonia, a short circuit in the biological nitrogen cycle that competes with denitrification." **FEMS Microbiology Ecology (49)**: 433-443.

Mortimer, R.J.G., S.J. Harris, M.D. Krom, T.E. Freitag, J.I. Prosser, J. Barnes, P. Anschutz, P.J. Hayes, and I.M. Davies (2004). "Anoxic nitrification in marine sediments." **Marine Ecology Progress Series (276)**: 37-51.

Mulder, A., A.A. van de Graaf, L.A. Robertson, J.G. Kuenen (1995). "Anaerobic ammonium oxidation discovered in a denitrifying fluidized bed reactor." **FEMS Microbiology Ecology (16)**: 177-184.

Neuhuber, S. M. U. (2003). In situ measurements of redox chemical species with amperometric techniques to investigate the dynamics of biogeochemical processes in aquatic systems. **Earth and Atmospheric Sciences**. Atlanta, Georgia Institute of Technology**:** 135.

Nordstrom, D.K., J.L. Munoz (1994). **Geochemical Thermodynamics**. Blackwell Scientific Publications, Inc., Cambridge, MA.

Perez-Benito, J. F., E. Brillas, R. Pouplana (1989). "Identification of a soluble form of colloidal manganese(IV)." **Inorganic Chemistry (28)**: 390-392.

Plus, M., A. Chapelle, P. Lazure, I. Auby, G. Levavasseur, M. Verlaque, T. Belsher, J.-M. Deslous-Paoli, J.-M. Zaldívar, C.N. Murray (2003). "Modelling of oxygen and nitrogen cycling as a function of macrophyte community in the Thau lagoon." **Continental Shelf Research (23)**: 1877-1898.

Risgaard-Peterson, N., R.L. Meyer, M. Schmid, M.S.M. Jetten, A. Enrich-Prast, S. Rysgaard, and N.P. Revsbech (2004). "Anaerobic ammonium oxidation in an estuarine sediment." **Aquatic Microbial Ecology (36)**: 293-304.

Rozan, T.F. and G.W. Luther (III) (2002). "An anion chromatography/ultraviolet detection method to determine nitrite, nitrate, and sulfide concentrations in saline (pore) waters." **Marine Chemistry (77)**: 1-6.

Straub, K.L., M. Benz, B. Schink, F. Widdel (1996). "Anaerobic, nitrate-dependent microbial oxidation of ferrous iron." **Applied and Environmental Microbiology (62)**: 1458-1460.

Straub, K.L., B.E.E. Buchholz-Cleven (1998). "Enumeration and detection of anaerobic ferrous iron-oxidizing, nitrate-reducing bacteria from diverse European sediments." **Applied and Environmental Microbiology (64)**: 4846-4856.

Strickland, J. D. H., T.R. Parsons (1972). **Practical Handbook of Seawater Analysis**. Ottawa, Fisheries Research Board of Canada.

Sutka, R.L., N.E. Ostrom, P.H. Ostrom, M.S. Phanikumar (2004). "Stable nitrogen isotope dynamics of dissolved nitrate in a transect from the North Pacific Subtropical Gyre to the Eastern Tropical North Pacific." **Geochimica et Cosmochimica Acta (68)**: 517-527.

Taillefert, M., G.W. Luther (III), and D.B. Nuzzio (2000). "The application of electrochemical tools for in situ measurements in aquatic systems." **Electroanalysis (12)**: 401-412.

Takeuchi, J (2006). "Habitat segregation of a functional gene encoding nitrate ammonification in estuarine sediments." **Geomicrobiology Journal (23)**: 75-87.

Tessier, A., P.G.C. Campbell, and M. Bisson (1979). "Sequential extraction procedure for the speciation of particulate trace metals." **Analytical Chemistry (51)**: 844-851.

Thamdrup, B., T. Dalsgaard (2000). "The fate of ammonium in anoxic manganese oxide-rich marine sediment." **Geochimica et Cosmochimica Acta (64)**: 4157-4164.

Thamdrup, B. and T. Dalsgard (2002). "Production of N_2 through anaerobic ammonium oxidation coupled to nitrate reduction in marine sediments." **Applied and Environmental Microbiology (68)**: 1312-1318.

Trimmer, M. J.C. Nicholls, B. Deflandre (2003). “Anaerobic ammonium oxidation measured in sediments along the Thames Estuary, United Kingdom.” **Applied and Environmental Microbiology (69)**: 6447-6454.

Vance-Harris, C., E. Ingall (2005). “Denitrification pathways and rates in the sandy sediments of the Georgia continental shelf, USA.” **Geochemical Transactions (6)**: 12-18.

Welsh, D.T., G. Castadelli (2004). “Bacterial nitrification activity directly associated with isolated benthic marine animals.” **Marine Biology (144)**: 1029-1037.